THE JOURNAL OF PHYSICAL CHEMISTRY A
A JOURNAL OF THE AMERICAN CHEMICAL SOCIETY

pubs.acs.org/JPCA

Article

Noncanonical Isomers of Nucleoside Cation Radicals: An Ab Initio Study of the Dark Matter of DNA Ionization

Shu R. Huang and František Tureček*

Cite This: J. Phys. Chem. A 2022, 126, 2480−2497

Read Online

ACCESS | Metrics & More | Article Recommendations | Supporting Information

ABSTRACT: Cation radicals of DNA nucleosides, 2′-deoxyadenosine, 2′-deoxyguanosine, 2′-deoxycytidine, and 2′-deoxythimidine, can exist in standard canonical forms or as noncanonical isomers in which the charge is introduced by protonation of the nucleobase, whereas the radical predominantly resides in the deoxyribose moiety. Density functional theory as well as correlated ab initio calculations with coupled clusters (CCSD(T)) that were extrapolated to the complete basis set limit showed that noncanonical nucleoside ion isomers were thermodynamically more stable than their canonical forms in both the gas phase and as water-solvated ions. This indicated the possibility of exothermic conversion of canonical to noncanonical forms. The noncanonical isomers were calculated to have very low adiabatic ion−electron recombination energies (RE_{ad}) for the lowest-energy isomers 2′-deoxy-(N-3*H*)adenos-1′-yl (4.74 eV), 2′-deoxy-(N-7*H*)guanos-1′-yl (4.66 eV), 2′-deoxy-(N-3*H*)cytid-1′-yl (5.12 eV), and 2′-deoxy-5-methylene-(O-2*H*)uridine (5.24 eV). These were substantially lower than the RE_{ad} value calculated for the canonical 2′-deoxyadenosine, 2′-deoxy guanosine, 2′-deoxy cytidine, and 2′-deoxy thymidine cation radicals, which were 7.82, 7.46, 8.14, and 8.20 eV, respectively, for the lowest-energy ion conformers of each type. Charge and spin distributions in noncovalent cation-radical dA⊂dT and dG⊂dC nucleoside pairs and dAT, dCT, dTC, and dGC dinucleotides were analyzed to elucidate the electronic structure of the cation radicals. Born−Oppenheimer molecular dynamics trajectory calculations of the dinucleotides and nucleoside pairs indicated rapid exothermic proton transfer from noncanonical $T^{+\cdot}$ to A in both $dAT^{+\cdot}$ and $dA⊂dT^{+\cdot}$, leading to charge and radical separation. Noncanonical $T^{+\cdot}$ in $dCT^{+\cdot}$ and $dTC^{+\cdot}$ initiated rapid proton transfer to cytosine, whereas the canonical $dCT^{+\cdot}$ dinucleotide ion retained the cation radical structure without isomerization. No spontaneous proton transfer was found in $dGC^{+\cdot}$ and $dG⊂dC^{+\cdot}$ containing canonical neutral and noncanonical ionized deoxycytidine.

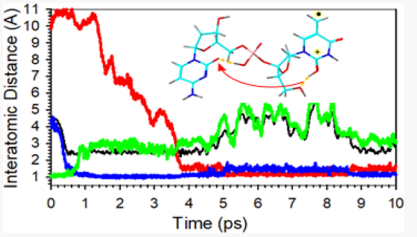

INTRODUCTION

Ionization of DNA by energetic elementary particles (α, β, protons, or γ-rays) is ubiquitous because of human exposure to radionuclides or high-altitude travel.[1−3] Direct DNA ionization creates an electron deficiency (called a "hole") that can propagate by electron transfer along the DNA strand or double helix, resulting eventually in chemical modifications of the nucleobases or deoxyribose moieties. Charge migration in oligonucleotide models of DNA has been studied extensively[4−6] using indirect ionization mediated by photoexcited components that were either intercalated in the oligonucleotide[7] or covalently tethered to it.[8,9] These studies have resulted in the current model of charge propagation that ranks the nucleobases by their ionization energies or redox potentials, concluding that most radical reactions occur at guanine as the most readily ionized nucleobase. However, studies of photoinduced ionization of nucleotides containing adenosine and thymidine have revealed radical reactions at thymine[10−14] which did not fit the hole migration model according to which adenine ionization by electron transfer should be expected. Ionization of DNA components has been addressed by numerous computational studies using density functional theory (DFT)[15−21] or wave function methods[22] including electron correlation.[23−32] These studies have provided accurate vertical and adiabatic ionization energies of standard nucleobases and approximate ionization energies of nucleosides and nucleotides. Structural changes in nucleobase cation radicals caused by ionization have been discussed for the standard (canonical) nucleobases.[15] Ionization of sugar-based C1′-C5′ nucleoside radicals has been addressed by DFT calculations.[21] In addition, recent experimental and computational studies addressed the dynamics of electronic excitation in nucleobase and nucleotide cation radicals at high levels of theory.[33−37] Recently, isomeric forms of nucleobase cation radicals have been discovered as stable gas-phase species and characterized by UV−visible photodissociation action spectroscopy.[38] The noncanonical isomer of the thymine cation radical, [4-hydroxy-5-methylene-(*1,3H*)pyrimid-2-one]$^{+\cdot}$, was formed as a major component, along with the canonical isomer, by electron transfer oxidation of thymine in a copper-

Received: February 6, 2022
Revised: April 5, 2022
Published: April 19, 2022

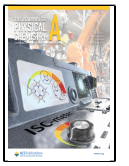

https://doi.org/10.1021/acs.jpca.2c00894
J. Phys. Chem. A 2022, 126, 2480−2497

Scheme 1. Structures and Atom Numbering in DNA Nucleosides

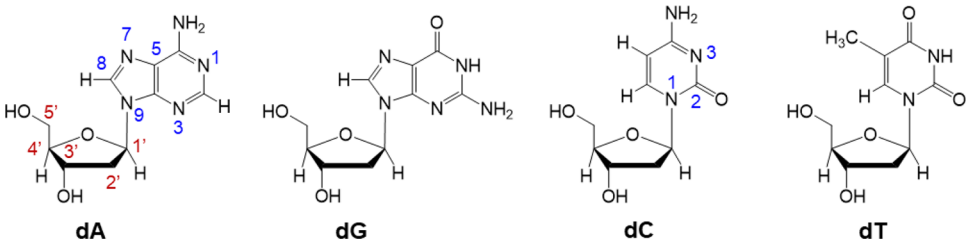

terpyridine complex.[39] The noncanonical isomer and its enol tautomers have been found by DFT[40] and ab initio coupled cluster CCSD(T) calculations to be thermodynamically more stable than the canonical thymine isomer.[39] Similarly, the noncanonical isomer of the 1-methylcytosine cation radical, [1-methylene-2-hydroxy-4-aminopyrimidine]$^{+\cdot}$, has been found to form spontaneously by electron transfer oxidation of 1-methylcytosine in a copper-terpyridine complex in the gas phase and was characterized spectroscopically.[41] Ab initio calculations at the CCSD(T)/ complete basis set (CBS) level of theory have indicated that the noncanonical 2-OH methylenecytosine cation radical and its N3-H-tautomer were 59 and 56 kJ mol^{-1} more stable, respectively, than the canonical form.[41] The noncanonical isomer of the 9-methyladenine cation radical, [9-methylene-(*1H*)adenine]$^{+\cdot}$, has been generated recently in the gas phase and calculated to be more stable than its canonical isomer.[42] The [9-methylene-(*1H*)adenine]$^{+\cdot}$ ion has been shown to have a distonic[43] electronic structure, whereby the radical and charge sites resided at different atoms.[44] An intriguing feature of the remarkably stable noncanonical cation radicals was that their neutral forms were high-energy isomers of the canonical nucleobases. This implied extremely low adiabatic ion−electron recombination energies for the noncanonical nucleobase cation radicals that were in the 5.7−5.9 eV range.[39,41,42] Because of their low recombination energies, noncanonical nucleobase cation radicals can be envisioned to trap the electron vacancy in ionized DNA and prevent hole migration. Calculations of adenosine cation radicals carried out at the CCSD(T)/CBS level of theory have indicated extremely low recombination energies of <5 eV for adenosine cation radical isomers.[42] Photoexcitation of ionized 2′-deoxyguanosine has been reported to produce distonic 2′-deoxyribose radicals,[45] and proton-transfer isomerizations of 2′-deoxyguanosine cation radicals have been studied by experiment[46] and DFT theory,[47] and the results have been debated.[48,49]

These previous results, showing the spontaneous or photoinduced formation of noncanonical nucleobase cation radicals and their low energies in the gas phase, warranted a comprehensive study of cation-radical isomers of the four DNA nucleosides (Scheme 1) to investigate the role of the deoxyribose moiety.

The paper is organized as follows. First, we present optimized structures and relative energies of cation radicals of 2′-deoxyadenosine (dA$^{+\cdot}$), 2′-deoxyguanosine (dG$^{+\cdot}$), 2′-deoxycytidine (dC$^{+\cdot}$), and 2′-deoxythymidine (dT$^{+\cdot}$) to compare the canonical and noncanonical forms. Next, we present and discuss the cation-radical recombination energies. Finally, we describe investigations of the energetics of proton transfer from noncanonical nucleosides and the dynamics of ionized nucleobase interactions in noncanonical thymidine and cytidine dinucleotides, dAT$^{+\cdot}$, dCT$^{+\cdot}$, dT$^{+\cdot}$C, and dGC$^{+\cdot}$, respectively, and noncovalent cation-radical nucleoside pairs, dA⊂dT$^{+\cdot}$ and dG⊂dC$^{+\cdot}$ where the symbol ⊂ denotes that the nucleosides are noncovalently bound.

CALCULATIONS

Born−Oppenheimer molecular dynamics (BOMD) calculations were performed using the Cuby4 high-level platform,[50,51] as described previously.[52] In brief, trajectories were run with PM6-D3H4[53] for 20 ps at 1 fs steps, starting from several initial configurations. This included both electron wave functions and nuclei thermal motion. The temperature was set at 510 K, employing the Berendsen thermostat to damp fluctuations of kinetic energy.[54] The trajectories consisting of 20,000 snapshots were sampled at regular intervals to extract 200 structures that were gradient-optimized with PM6-D3H4 using MOPAC.[55] The optimized structures were compacted to sort out duplicates, and 20−30 structures were selected for further geometry optimizations. These were performed with B3LYP[56] and M06-2X[57] hybrid DFT methods using the 6−31 + G(d,p) basis set. B3LYP/6−31 + G(d,p) was used to calculate harmonic frequencies that were scaled by 0.975 and used to obtain zero-point vibrational energies, enthalpies, and entropies at 310 K. Entropy corrections due to hindered rotors were applied.[58] The spin-unrestricted formalism was used for all odd-electron species, such as cation radicals and neutral radicals. The M06-2X/6−31 + G(d,p)-optimized geometries were used for single-point energy calculations. These were carried out with M06-2X/6−311++G(2d,p) for all species. Additionally, we ran ab initio calculations with Møller−Plesset theory truncated at the second order and with valence-electron-only excitations, MP2(frozen core), and the correlation consistent basis sets, aug-cc-pVDZ, aug-cc-pVTZ, and aug-cc-pVQZ.[59] The quadruple ζ calculations required over 6 Tbytes of scratch space. Spin contamination in the Hartree−Fock and MP2 calculations was handled by a spin annihilation precedure.[60,61] The Hartree−Fock and MP2 energies were used to extrapolate the electron correlation energy to the CBS, using the formula $E_{corr} = a + bX^{-3}$ where X is the ζ split in the aug-cc-pVXZ basis set.[62] The *a* and *b* values are summarized in Table S1 (Supporting Information). In addition, coupled cluster[63] single-point energy calculations were carried out with single, double, and disconnected triple excitations, CCSD(T),[64] using the aug-cc-pVDZ basis set. The single-point energies were combined to produce extrapolated CCSD(T)/CBS energies according to the formula

$$\text{CCSD(T)/CBS} \approx \text{CCSD(T)/aug-cc-pVDZ} - \text{MP2/aug-cc-pVDZ} + \text{HF/aug-cc-pVQZ} + E_{\text{corr}\to\infty}$$

We did not extrapolate HF energies to the CBS,[65] as the combinations of HF/aug-cc-pVXZ energies showed occasional irregularities. Using UHF/UMP2 and spin-projected HF/MP2 energies resulted in <0.0003 Hartree (<0.8 kJ mol^{-1}) differences in the final

https://doi.org/10.1021/acs.jpca.2c00894
J. Phys. Chem. A 2022, 126, 2480−2497

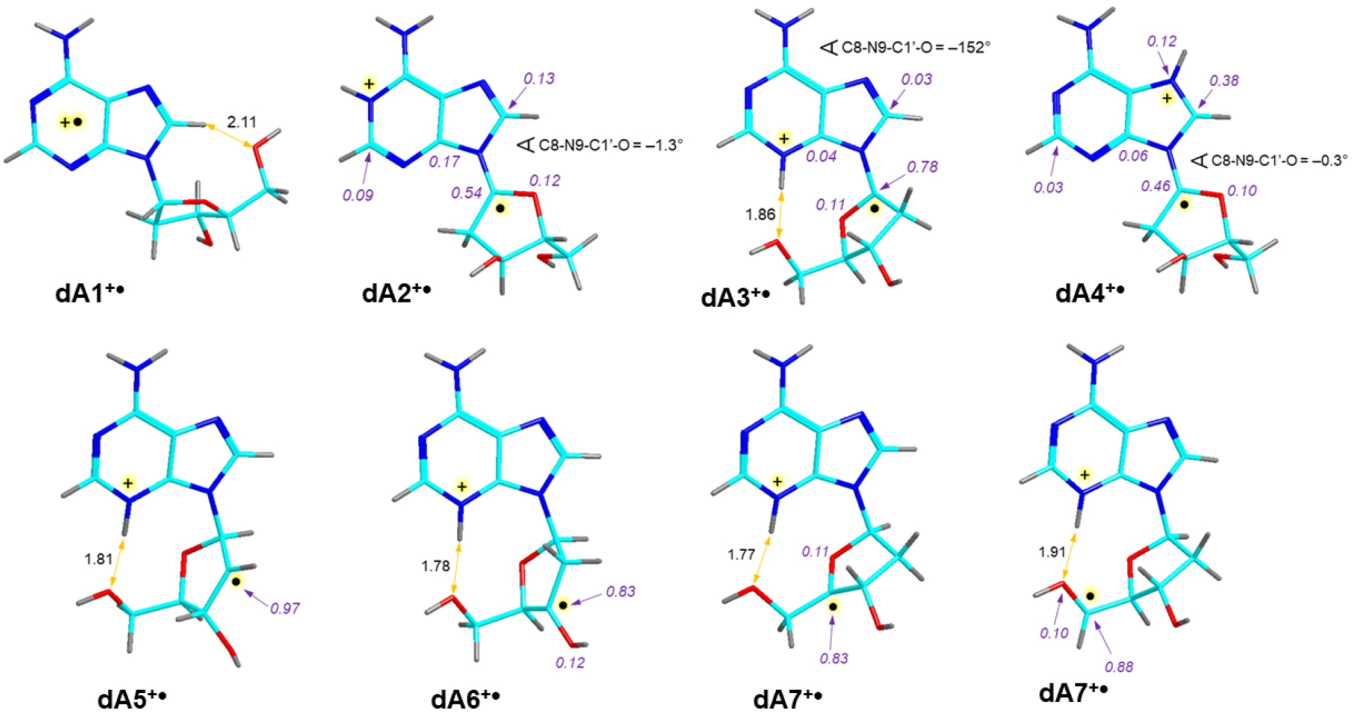

Figure 1. M06-2X/6−31 + G(d,p)-optimized structures of 2′-adenosine cation radicals. Yellow double-headed arrows indicate hydrogen bonds with distances in Ångstrøms. Purple italics represent NPA atomic spin densities.

Table 1. Relative Energies of 2′-Deoxyadenosine Cation Radical Isomers

	relative energy[ab]			
ion	M06-2X/6−31 + G(d,p)	M06-2X/6−311++G(2d,p)[c]	CCSD(T)/aug-cc-pVTZ[cd]	CCSD(T)/CBS[e]
dA1$^{+\cdot}$	0.0 (0.0)[f] (0.0)[g]	0.0 (0.0)[g]	0.0	0.0
dA2$^{+\cdot}$	−26 (−29)[f] (−43)[g]	−26 (−42)[g]	−16	−18
dA3$^{+\cdot}$	−44 (−42)[f] (−38)[g]	−41 (−35)[g]	−39	−40
dA4$^{+\cdot}$	−22 (−26)[f] (−32)[g]	−23 (−33)[g]	−13	−15
dA5$^{+\cdot}$	−21 (−19)[f] (−19)[g]	−17 (−16)[g]		
dA6$^{+\cdot}$	−41 (−41)[f] (−40)[g]	−38 (−37)[g]	−36	−37
dA7$^{+\cdot}$	−31 (−32)[f] (−33)[g]	−29 (−30)[g]		
dA8$^{+\cdot}$	−30 (−29)[f] (−33)[g]	−26 (−29)[g]		

[a]In kJ mol^{-1}. [b]Including scaled B3LYP/6−31 + G(d,p) zero-point energies and referring to 0 K unless stated otherwise. [c]Single-point energies on M06-2X/6−31 + G(d,p)-optimized geometries. [d]From linear basis set expansion: E[CCSD(T)/aug-cc-pVTZ] ≅ E[CCSD(T)/aug-cc-pVDZ] + E[MP2/aug-cc-pVTZ] − E[MP2/aug-cc-pVDZ]. [e]Correlation energy extrapolated to the CBS. [f]Relative Gibbs energies at 310 K. [g]Relative Gibbs energies at 310 K in water dielectric.

CCSD(T)/CBS energies. Atomic charges and spin densities were calculated by natural population analysis (NPA)[66] of M06-2X/6−311++G(2d,p) wave functions. Solvation energies were estimated by self-consistent reaction field calculations using the polarizable continuum model (PCM)[67] and water dielectric constant. Solvated structures were fully optimized with PCM-M06-2X/6−31 + G(d,p) and PCM-M06-2X/6−311++G(2d,p). All ab initio and DFT calculations were carried out using Gaussian 16, Revision A03.[68]

RESULTS AND DISCUSSION

2′-Deoxyadenosine. Calculations of adenosine cation radicals have been mentioned previously[42] and are expanded and discussed here for the sake of completeness. The lowest-energy conformer of the canonical isomer **dA1**$^{+\cdot}$ showed an optimized structure that followed that of the neutral nucleoside (Figure 1, Table S2, Supporting Information). Ionization resulted in alternating bond length changes, elongating the C2−N3, C4−C5, C5−C6, N7−C8, and N9−C1′ bonds, while shortening the N1−C2, C6−N10, C5−N7, C8−N9, and C1′−O bonds. The changes in the adenine bond lengths were similar to those reported by Improta et al. for adenine,[15] except for the N1−C2 bond which was elongated according to our M06-2X optimization, while it was contracted according to the previous B1LYP geometry optimization.[15] Structure **dA1**$^{+\cdot}$ showed a nonbonding interaction between H8 and the 5′-O hydroxyl at 2.11 Å that can be viewed as a weak hydrogen bond of the acidic H8. Ion **dA1**$^{+\cdot}$ had >99% of spin density in the adenine ring, according to natural population analysis of the M06-2X/6−311++G(2d,p) molecular orbitals. Noncanonical isomers were constructed by moving a hydrogen atom from C1′ to the basic N1, N3, and N7 positions in adenine, resulting in tautomers **dA2**$^{+\cdot}$, **dA3**$^{+\cdot}$, and **dA4**$^{+\cdot}$, respectively. The lowest-energy conformers of each tautomer group of the noncanonical isomers are shown in Figure 1. The noncanonical

https://doi.org/10.1021/acs.jpca.2c00894
J. Phys. Chem. A 2022, 126, 2480−2497

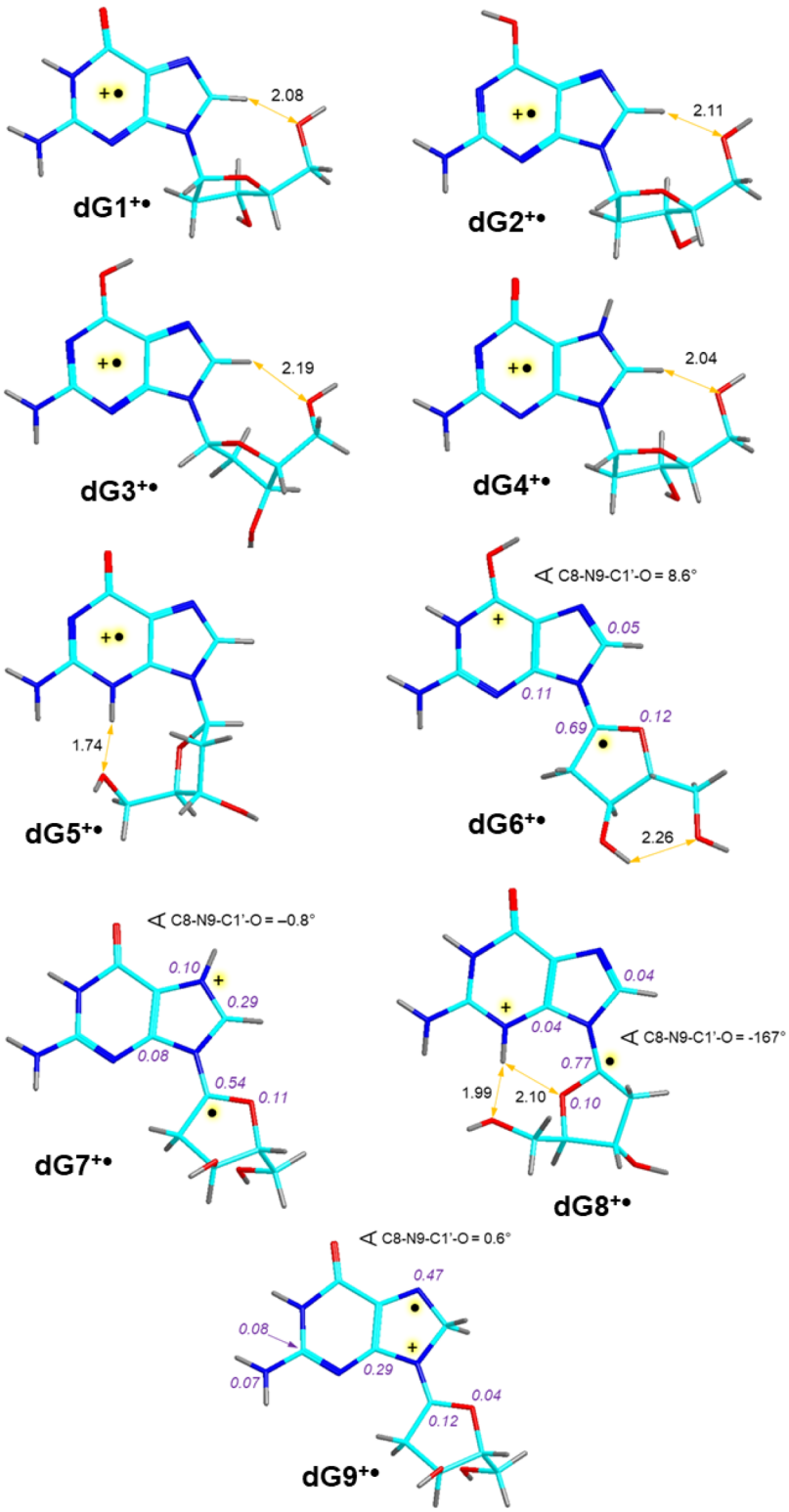

Figure 2. M06-2X/6−31 + G(d,p)-optimized structures of 2′-deoxyguanosine cation radicals. Description as in Figure 1.

isomers showed different dihedral angles about the C1′−N9 bond connecting the deoxyribose and adenine rings, which affected electron interaction between the radical-carrying C1′ and the adenine π-electronic system. Structures **dA2**$^{+\bullet}$ and **dA4**$^{+\bullet}$ had essentially coplanar arrangements of the rings, as evidenced by small C8−N9−C1′−O dihedral angles, resulting in spin delocalization to the adenine imidazole atoms (Figure 1). The lowest-energy tautomer **dA3**$^{+\bullet}$ was stabilized by a hydrogen bond between N3-H and 5′-O which was accompanied by a 28 degree twist about the C1′−N9 bond. This tautomer showed the highest spin density at the deoxyribose C-1′ and ring oxygen atoms (Figure 1). Placing the radical on C1′ resulted in a substantial stabilization of the 2′-deoxyadenosine cation radicals that reached −40 kJ mol^{-1} in **dA3**$^{+\bullet}$ relative to the canonical isomer **dA1**$^{+\bullet}$ (Table 1). The stabilization of the N3-H tautomer **dA3**$^{+\bullet}$ relative to **dA2**$^{+\bullet}$ and

https://doi.org/10.1021/acs.jpca.2c00894
J. Phys. Chem. A 2022, 126, 2480−2497

Table 2. Relative Energies of 2′-Deoxyguanosine Cation Radical Isomers

	relative energy[a,b]			
ion	M06-2X/6−31 + G(d,p)	M06-2X/6−311++G(2d,p)[c]	CCSD(T)/aug-cc-pVTZ[c,d]	CCSD(T)/CBS[e]
dG1$^{+\bullet}$	0.0 (0.0)[f] (0.0)[g]	0.0 (0.0)[g]	0.0	0.0
dG2$^{+\bullet}$	2.3 (0.7) (29)[g]	1.0 (28)[g]	2.3	0.8
dG3$^{+\bullet}$	7.0 (8.2) (38)[g]	4.5 (36)[g]	5.0	3.6
dG4$^{+\bullet}$	51 (52) (45)[g]	50 (45)[g]	46	47
dG5$^{+\bullet}$	11 (73) (43)[g]	69 (42)[g]	62	64
dG6$^{+\bullet}$	19 (16) (40)[g]	18 (36)[g]	25	22
dG7$^{+\bullet}$	−19 (−22) (−2)[g]	−18 (−0.7)[g]	−10	−13
dG8$^{+\bullet}$	37 (37) (12)[g]	38 (13)[g]	38	36
dG9$^{+\bullet}$	−4.5 (−5.4) (−2.2)[g]	−6.8 (−4.8)[g]	−4.2	−4.6

[a]In kJ mol^{-1}. [b]Including scaled B3LYP/6−31 + G(d,p) zero-point energies and referring to 0 K unless stated otherwise. [c]Single-point energies on M06-2X/6−31 + G(d,p)-optimized geometries. [d]From linear basis set expansion: E[CCSD(T)/aug-cc-pVTZ] ≅ E[CCSD(T)/aug-cc-pVDZ] + E[MP2/aug-cc-pVTZ] − E[MP2/aug-cc-pVDZ]. [e]Correlation energy extrapolated to the CBS. [f]Values in parentheses are relative Gibbs energies at 310 K. [g]Relative Gibbs energies at 310 K in water dielectric.

dA4$^{+\bullet}$ was analogous to that of protonated 2′-deoxyadenosine that also preferred an N3-H tautomer.[69] We note that the ranking of the M06-2X relative energies for **dA1**$^{+\bullet}$-**dA4**$^{+\bullet}$ closely followed that from CCSD(T) calculations with large basis sets, placing **dA3**$^{+\bullet}$ as the lowest-energy isomer (Table 1). Solvation by water was investigated by PCM calculations with full geometry optimization with M06-2X/6−31 + G(d,p) and M06-2X/6−311++G(2d,p). The calculated energies (Table 1) showed stabilization of the noncanonical isomers relative to **dA1**$^{+\bullet}$ that was of a similar magnitude to that in the gas phase. The noncanonical N1-H tautomer **dA2**$^{+\bullet}$ was the lowest free-energy solvated cation radical by a small margin among those studied.

The reason for the greater thermodynamic stability of the noncanonical 2′-deoxyadenosine cation radicals **dA2**$^{+\bullet}$-**dA4**$^{+\bullet}$ relative to **dA1**$^{+\bullet}$ can be traced to the bond dissociation energies of the differentiating C−H and N−H bonds. For example, isomerization of **dA1**$^{+\bullet}$ to **dA2**$^{+\bullet}$ comprises homolytic cleavage of the nonpolar C1′−H bond and formation of the polar N1−H bond. The difference between the pertinent bond energies, plus relaxation of the other bond lengths and angles, then determines the enthalpy change. Isomerizations of this type where a nonpolar C−H bond is replaced by a polar X−H bond often result in stabilization of cation radicals, as first reported by Radom and co-workers for distonic ions of the $^{\cdot}CH_2XH^+$ type, where X = O, N.[43] The well-known stabilization of simple enol cation radicals relative to their aldehyde and ketone isomers is also well documented.[70−73] With **dA3**$^{+\bullet}$, the noncanonical structure gains further stabilization because of the hydrogen bond to O5. The stabilizing C to N hydrogen transfer can be applied to the other C−H bonds in 2′-deoxyadenosine cation radicals. This is illustrated by the C2′, C3′, C4′, and C5′ radicals, **dA5**$^{+\bullet}$-**dA8**$^{+\bullet}$, respectively, that are all thermodynamically more stable than **dA1**$^{+\bullet}$ (Table 1). The interaction of the C-based radical with *n*-type electrons at the adjacent oxygen atom appears to have only a minor effect, stabilizing the C3′, C4′, and C5′ radicals relative to the C2′ radical **dA5**$^{+\bullet}$. This interaction resulted in a transfer of 10−12% spin density from the carbon atom to the adjacent oxygen atom in **dA6**$^{+\bullet}$-**dA8**$^{+\bullet}$ (Figure 1).

2′-Deoxyguanosine. Both the canonical and noncanonical 2′-deoxyguanosine cation radicals can be realized in several tautomers whose structures were investigated including full conformational analysis. The lowest-energy conformers of each tautomer are shown in Figure 2, and their relative energies are listed in Table 2. Structures **dG1**$^{+\bullet}$-**dG5**$^{+\bullet}$ are guanine isomers of which the N1-H (**dG1**$^{+\bullet}$) and O-H tautomers (**dG2**$^{+\bullet}$) were virtually isoenergetic in the gas phase at all levels of theory used herein (Table 2). The O-H rotamer **dG3**$^{+\bullet}$ was slightly less stable than **dG1**$^{+\bullet}$ and **dG2**$^{+\bullet}$. Solvation by water significantly favored the N1-H tautomer **dG1**$^{+\bullet}$ which was 28 kJ mol^{-1} more stable than solvated **dG2**$^{+\bullet}$ (Table 2). The N7-H and N3-H tautomers, **dG4**$^{+\bullet}$ and **dG5**$^{+\bullet}$, respectively, had notably higher relative energies than **dG1**$^{+\bullet}$ and **dG2**$^{+\bullet}$ in both the gas phase and water dielectric, consistent with previous DFT calculations.[47] Out of the noncanonical isomers, the N1, N7-H tautomer **dG7**$^{+\bullet}$ was the global energy minimum in the gas phase at −13 kJ mol^{-1} relative to **dG1**$^{+\bullet}$. This difference was diminished to −0.7 kJ mol^{-1} by solvation in water dielectric (Table 2). Remarkably, the N1-H, O-H tautomer **dG6**$^{+\bullet}$, which is the noncanonical C1′ radical analogue of **dG3**$^{+\bullet}$, was destabilized by 35 kJ mol^{-1} relative to **dG7**$^{+\bullet}$ (Table 2). The noncanonical N1, N3-H tautomer with a C1′ radical (**dG8**$^{+\bullet}$) was less stable than **dG1**$^{+\bullet}$. Finally, the C8-dihydroguanine isomer **dG9**$^{+\bullet}$ was marginally more stable than **dG1**$^{+\bullet}$.

The relative energies of the canonical and noncanonical isomers showed different trends. In the canonical series, **dG1**$^{+\bullet}$-**dG5**$^{+\bullet}$, the relative energies of the 2′-deoxyguanine cation radicals followed those of guanine cation radicals where the lowest-energy cation-radical tautomer[74] corresponds to ionization of the lowest energy neutral guanine.[75,76] In contrast, the ranking of the noncanonical cation-radical energies, **dG6**$^{+\bullet}$-**dG8**$^{+\bullet}$, was consistent with that reported for closed-shell 2′-deoxyguanosine cations where the N3-H protonated tautomer was the lowest-energy structure.[77] The substantial destabilization of the N1-H, O-H tautomer **dG6**$^{+\bullet}$ relative to the N1-H, N7-H tautomer **dG8**$^{+\bullet}$ is similar to that for protonated guanine tautomers where the N1-H, O-H, N9-H ion has been calculated by Colominas et al. to be 21 kJ mol^{-1} less stable than the N1-H, N7-H, N9-H global energy minimum.[78] These features, along with the prevalent localization of spin density at C1′ in **dG6**$^{+\bullet}$-**dG8**$^{+\bullet}$, indicated that the radical interacted only weakly with the π-electron system of protonated guanine. We note that a hydrated distonic 2′-deoxyguanosine cation radical with N7-protonated guanine and a C5′ radical defect has been calculated to be 54 kJ mol^{-1} more stable than the hydrated canonical isomer.[47]

2′-Deoxycytidine. Several isomers of 2′-deoxycytidine cation radicals were investigated, including canonical structures

https://doi.org/10.1021/acs.jpca.2c00894
J. Phys. Chem. A 2022, 126, 2480−2497

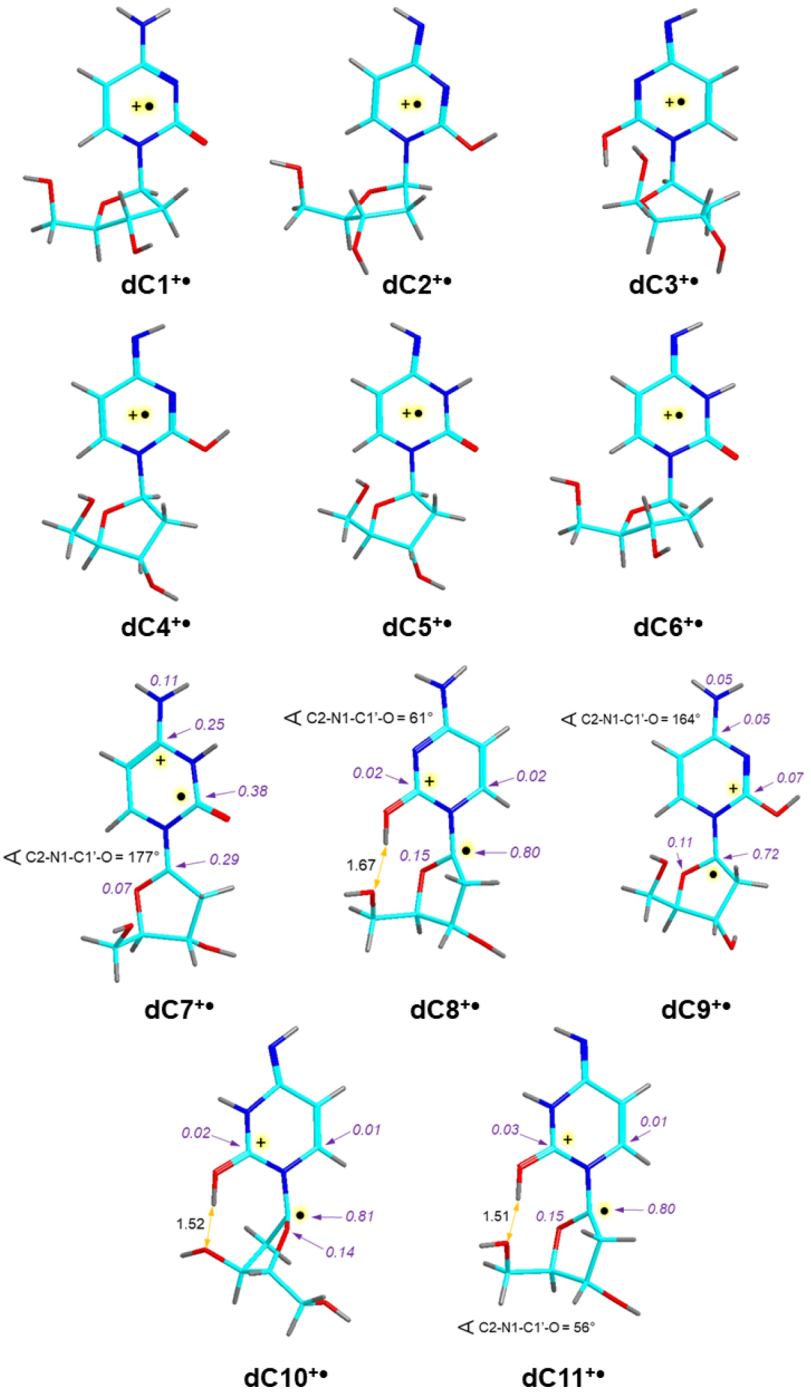

Figure 3. M06-2X/6−31 + G(d,p)-optimized structures of 2′-deoxycytidine cation radicals. Description as in Figure 1.

in which the electron defect was confined in the nucleobase (**dC1**$^{+\bullet}$-**dC6**$^{+\bullet}$), as well as distonic structures with the radical site at C1′ (**dC7**$^{+\bullet}$-**dC11**$^{+\bullet}$, Figure 3). Among the canonical structures, the lowest energy isomer was the 2-oxo, N3-H, 4-imine cation radical **dC5**$^{+\bullet}$ that was marginally more stable than the classical 2-oxo, 4-NH_2 cation-radical **dC1**$^{+\bullet}$ (Table 3). This order of thermodynamic stability was similar to that reported for analogous cytosine cation radicals carrying H or a methyl group at N-1.[24,41] Three of the noncanonical cation radicals, **dC7**$^{+\bullet}$-**dC9**$^{+\bullet}$, were found to be substantially more stable than the canonical forms (Table 3, Figure 3). The lowest-energy structure **dC7**$^{+\bullet}$ was an N3-H cytosine tautomer which showed a near-coplanar arrangement of the deoxyribose and cytosine rings, as illustrated by the C2−N1−C1′−O dihedral angle (Figure 3). This coplanarity allowed for a substantial delocalization of spin density, flowing from C1′ (29%) to the cytosine ring positions C2 (38%), C4 (25%), and the NH_2 group (11%). The other two low-energy isomers, **dC8**$^{+\bullet}$ and **dC9**$^{+\bullet}$, which were O2-H enol cytosine tautomers, displayed smaller C2−N1−C1′−O dihedral angles, resulting in spin density being localized at C1′. The ring twist in the second lowest-energy structure (**dC8**$^{+\bullet}$) was enforced by a hydrogen bond between the O2 hydroxyl and O5′ at 1.67 Å (Figure 3). The noncanonical cytosine N3-H, 4-imine tautomers (**dC8**$^{+\bullet}$ and **dC9**$^{+\bullet}$) were less stable than **dC7**$^{+\bullet}$ while still being substantially more stable than **dC1**$^{+\bullet}$. It is

https://doi.org/10.1021/acs.jpca.2c00894
J. Phys. Chem. A 2022, 126, 2480−2497

Table 3. Relative Energies of 2′-Deoxycytidine Cation Radical Isomers

	relative energy[ab]			
ion	M06-2X/6−31 + G(d,p)	M06-2X/6−311++G(2d,p)[c]	CCSD(T)/aug-cc-pVTZ[cd]	CCSD(T)/CBS[e]
dC1$^{+\bullet}$	0.0 (0.0)[f] (0.0)[g]	0.0 (0.0)[g]	0.0	0.0
dC2$^{+\bullet}$	41 (43)	42	40	41
dC3$^{+\bullet}$	72 (73)	72	67	69
dC4$^{+\bullet}$	18 (18)	21	23	23
dC5$^{+\bullet}$	−0.3 (−1.0) (6.0)[g]	1.1(5.7)[g]	−4.4	−3.1
dC6$^{+\bullet}$	6.3 (7.5) (7.1)[g]	7.9 (6.6)[g]	2.3	2.7
dC7$^{+\bullet}$	−95 (−96) (−69)[g]	−94 (−69)[g]	−80	−84
dC8$^{+\bullet}$	−74 (−72) (−45)[g]	−71(−44)[g]	−62	−64
dC9$^{+\bullet}$	−72 (−74) (−45)[g]	−69 (−45)[g]	−57	−60
dC10$^{+\bullet}$	1.0 (3.6) (31)[g]	5.1 (30)[g]	8.6	6.9
dC11$^{+\bullet}$	12 (15) (9.5)[g]	15 (8.0)[g]	18	16

[a]In kJ mol^{-1}. [b]Including scaled B3LYP/6−31 + G(d,p) zero-point energies and referring to 0 K unless stated otherwise. [c]Single-point energies on M06-2X/6−31 + G(d,p)-optimized geometries. [d]From linear basis set expansion: E[CCSD(T)/aug-cc-pVTZ] ≅ E[CCSD(T)/aug-cc-pVDZ] + E[MP2/aug-cc-pVTZ] − E[MP2/aug-cc-pVDZ]. [e]Correlation energy extrapolated to the CBS. [f]Values in parentheses are relative Gibbs energies at 310 K. [g]Relative Gibbs energies at 310 K in water dielectric.

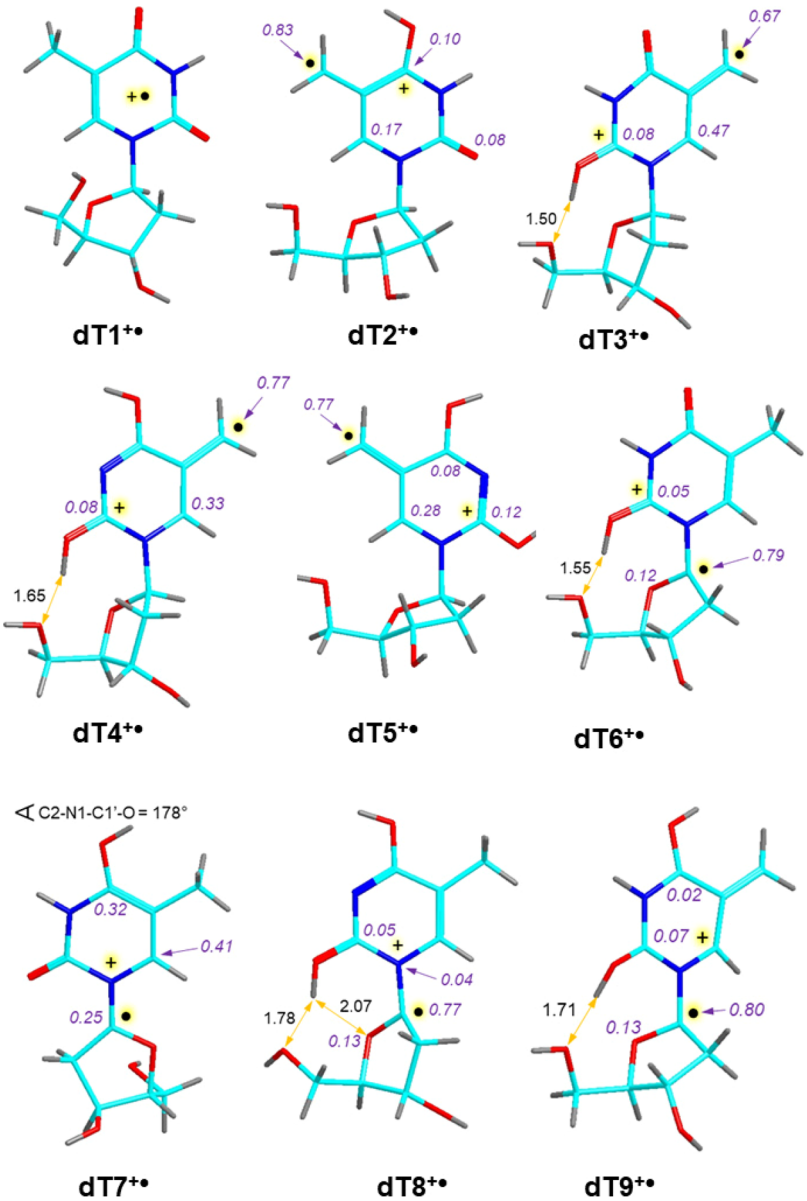

Figure 4. M06-2X/6−31 + G(d,p)-optimized structurers of 2′-deoxythymidine cation radicals. Description as in Figure 1.

https://doi.org/10.1021/acs.jpca.2c00894
J. Phys. Chem. A 2022, 126, 2480−2497

Table 4. Relative Energies of 2′-Deoxythymidine Cation Radical Isomers

	relative energy[ab]			
ion	M06-2X/6−31 + G(d,p)	M06-2X/6−311++G(2d,p)[c]	CCSD(T)/aug-cc-pVTZ[cd]	CCSD(T)/CBS[e]
dT1$^{+\cdot}$	0.0 (0.0)[f] (0.0)[g]	0.0	0.0	0.0
dT2$^{+\cdot}$	9.8 (14) (18)[g]	9.1	8.8	6.6
dT3$^{+\cdot}$	−18 (−11) (−2.6)[g]	−14	−13	−14
dT4$^{+\cdot}$	−12 (−3.7) (19)[g]	−11	−9.0	−11
dT5$^{+\cdot}$	−9.4 (−3.9) (20)[g]	−8.1	−2.8	−5.2
dT6$^{+\cdot}$	2.3 (6.5) (15)[g]	5.8	8.1	5.4
dT7$^{+\cdot}$	−18 (−16) (8.1)[g]	−19	−10	−14
dT8$^{+\cdot}$	28 (30) (42)[g]	27		
dT9$^{+\cdot}$	248 (251)	248		

[a]In kJ mol^{-1}. [b]Including scaled B3LYP/6−31 + G(d,p) zero-point energies and referring to 0 K unless stated otherwise. [c]Single-point energies on M06-2X/6−31 + G(d,p)-optimized geometries. [d]From linear basis set expansion: E[CCSD(T)/aug-cc-pVTZ] ≅ E[CCSD(T)/aug-cc-pVDZ] + E[MP2/aug-cc-pVTZ] − E[MP2/aug-cc-pVDZ]. [e]Correlation energy extrapolated to the CBS. [f]Values in parentheses are relative Gibbs energies at 310 K. [g]Relative Gibbs energies at 310 K in water dielectric.

Table 5. Adiabatic Recombination Energies of Nucleoside Cation Radical Isomers

	recombination energy[ab]			
ion	M06-2X/6−31 + G(d,p)	M06-2X/6−311++G(2d,p)[c]	CCSD(T)/aug-cc-pVTZ[cd]	CCSD(T)/CBS[e]
dA1$^{+\cdot}$	7.77 (6.28)[f]	7.76 (6.26)[f]	7.75	7.82
dA2$^{+\cdot}$	4.09 (3.16)[f]	4.12 (3.17)[f]	4.36	4.42
dA3$^{+\cdot}$	4.64 (3.46)[f]	4.65 (3.46)[f]	4.69	4.74
dA4$^{+\cdot}$	4.81 (3.23)[f]	4.88 (3.29)[f]	5.06	5.10
dG1$^{+\cdot}$	7.38	7.38	7.39	7.46
dG2$^{+\cdot}$	7.42	7.41	7.42	7.49
dG3$^{+\cdot}$	7.49	7.47	7.47	7.54
dG4$^{+\cdot}$	7.26	7.25	7.22	7.30
dG5$^{+\cdot}$	7.56	7.56	7.53	7.62
dG6$^{+\cdot}$	4.28 (4.20)[g]	4.30 (4.22)[g]	4.44	4.49
dG7$^{+\cdot}$	4.45	4.48	4.60	4.66
dG8$^{+\cdot}$	4.93	4.93	4.96	5.00
dG9$^{+\cdot}$	5.25	5.27	5.36	5.43
dC1$^{+\cdot}$	8.10	8.10	8.06	8.14
dC7$^{+\cdot}$	4.87	4.89	5.06	5.12
dC8$^{+\cdot}$	4.77	4.79	4.87	4.93
dC9$^{+\cdot}$	4.79	4.80	4.99	5.06
dT1$^{+\cdot}$	8.10	8.10	8.12	8.20
dT3$^{+\cdot}$	5.10	5.15	5.17	5.24
dT5$^{+\cdot}$	5.15	5.18	5.23	5.30
dT6$^{+\cdot}$	5.17	5.19	5.26	5.31
dT7$^{+\cdot}$	4.88	4.90	5.05	5.12

[a]Absolute values in eV. [b]Including scaled B3LYP/6−31 + G(d,p) zero-point energies and referring to 0 K. [c]Single-point energies on M06-2X/6−31 + G(d,p)-optimized geometries. [d]From linear basis set expansion: E[CCSD(T)/aug-cc-pVTZ] ≅ E[CCSD(T)/aug-cc-pVDZ] + E[MP2/aug-cc-pVTZ] − E[MP2/aug-cc-pVDZ]. [e]Correlation energy extrapolated to the CBS. [f]Adiabatic recombination energies in water dielectric. [g]Relative to neutral diradical triplet state.

noteworthy that the stabilization of the C1′ radicals **dC7**$^{+\cdot}$ and **dC8**$^{+\cdot}$ relative to the canonical isomer **dC1**$^{+\cdot}$ was greater than that reported for 1-methylcytosine cation radical isomers.[41] This may indicate stabilizing interactions of the C1′ radical with the flanking C2′ methylene and oxygen molecular orbitals in the deoxyribose ring.

2′-Deoxythymidine. The presence of the 5-methyl group in thymine gives rise to several noncanonical structures for 2′-deoxythymidine cation radicals in which either a 5-methyl hydrogen, H1′, or both were moved to the ring heteroatoms (Figure 4). Among isomers with the 5-methylene group (**dT2**$^{+\cdot}$-**dT5**$^{+\cdot}$), the lowest energy was found for the O2-H enol (**dT3**$^{+\cdot}$) at −13 kJ mol^{-1} relative to the canonical cation radical **dT1**$^{+\cdot}$ (Table 4). The O2 enol group was also stabilizing in the O2, O4 dienol structure **dT4**$^{+\cdot}$, possibly because of hydrogen bonding to the deoxyribose O5′ (Figure 4). The energy ranking of the 2′-deoxycytidine cation radical isomers was similar to that reported for thymine ions.[39] Moving the hydrogen atom from C1′ to O2 was slightly endergonic in the noncanonical O2-enol isomers as represented by the lowest-energy conformer **dT6**$^{+\cdot}$ (Table 4). This ion developed a strong hydrogen bond between O2-H and O5′ at 1.55 Å, which forced a thymine ring rotation to adapt a 37° dihedral angle about the C2−N1−C1′−O bond. The noncoplanar geometry was consistent with 79% spin density localization at C1′ and a 12% carryover to the deoxyribose ring oxygen. In contrast, among the noncanonical O4-enol C1′-radical tautomers, the lowest-energy conformer **dT7**$^{+\cdot}$ was the global

https://doi.org/10.1021/acs.jpca.2c00894
J. Phys. Chem. A 2022, 126, 2480−2497

energy minimum in the gas phase (Table 4). Ion **dT7**$^{+\cdot}$ had a coplanar arrangement of the thymine and deoxyribose rings (Figure 4) that allowed the unpair electron density to be delocalized among the C1′, C4, and C6 positions. However, enolization at both O2 and O4 was energetically unfavorable in the C1′ radical **dT8**$^{+\cdot}$ in which the O2-H hydrogen bond to O5′ again forced a thymine ring rotation. Finally, a further isomerization in **dT6**$^{+\cdot}$ by moving the 5-methyl hydrogen to O4 was associated with a steep energy increase (+242 kJ mol^{-1}, Table 4) in the noncanonical isomer **dT9**$^{+\cdot}$.

These results indicated that thymidine cation-radical stabilization was due to a large part to the expansion of the π-electronic system by including the exocyclic 5-methylene, as in **dT3**$^{+\cdot}$-**dT5**$^{+\cdot}$, or C1′ as in **dT7**$^{+\cdot}$. This electronic effect was more strongly stabilizing than the hydrogen bond between O2-H and O5′ in **dT6**$^{+\cdot}$ and **dT8**$^{+\cdot}$. It is noteworthy that solvation with water, as approximated by the polarized dielectric PCM, was most stabilizing in the canonical isomer **dT1**$^{+\cdot}$ which showed the largest solvation energy at −217 kJ mol^{-1}. Among the noncanonical isomers, only **dT3**$^{+\cdot}$ had a lower energy than **dT1**$^{+\cdot}$ when solvated in water dielectric, whereas the other noncanonical isomers were relatively disfavored when polar interactions with the solvent were included. We note that the PCM does not deal with specific interactions between the ion and surrounding solvent molecules, and more sophisticated methods based on a QM:QM approach may be necessary to obtain deeper insight into the solvent effects.[79]

Recombination Energies. The direction of spontaneous electron transfer in ionized DNA depends on the energy levels of the relevant frontier molecular orbitals in the nucleobases. These are typically approximated by the recombination energies of the nucleobase cation radicals which, if taken as adiabatic absolute values ($|RE_{ad}|$), are equal to the nucleobase adiabatic ionization energies. We calculated the adiabatic recombination energies of several representative nucleoside cation radicals for both the canonical and noncanonical forms of dA$^{+\cdot}$, dG$^{+\cdot}$, dC$^{+\cdot}$, and dT$^{+\cdot}$. Electron attachment to the canonical isomers, followed by geometry relaxation, yielded singlet states, as shown for **dA1**$^{+\cdot}$ (Scheme S1, Supporting Information). With the noncanonical isomers, electron attachment can produce singlet (sg) or triplet (tp) states with tricoordinate C1′ (Schemes S2−S4, SI). Adenine noncanonical isomers **dA2**-**dA4** were calculated to be more stable as singlet states, which was shown by their higher $|RE_{ad}|$ compared to those forming the neutral triplets.

The $|RE_{ad}|$ of **dA1**$^{+\cdot}$ (7.82 eV, Table 5) was nearly identical to the adiabatic ionization energy of adenosine reported previously by Pluhařová et al. on the basis of their DFT calculations.[19] Solvation by water substantially lowered the $|RE_{ad}|$ of **dA1**$^{+\cdot}$ to 6.26 eV, again in agreement with the previously reported ionization energy.[19] The conspicuous feature of electron recombination with **dA2**$^{+\cdot}$-**dA4**$^{+\cdot}$ was the formation of neutral forms **dA2**-**dA4** that were 247−309 kJ mol^{-1} less stable than **dA1** (Table S3, Supporting Information) that resulted in lower $|RE_{ad}|$ for all these ions. Reduction of the lowest energy N3-H tautomer **dA3**$^{+\cdot}$ was associated with $|RE_{ad}|$ = 4.74 eV which was bracketed by the $|RE_{ad}|$ values for **dA2**$^{+\cdot}$ and **dA4**$^{+\cdot}$ at 4.42 and 5.10 eV, respectively (Table 5). The resulting neutral adenosines were high-energy isomers of the canonical form **dA1**, as shown by the calculated relative energies in Table S3. Neutral **dA2**(sg) had a planar purine ring system with a very minor pyramidization of the NH_2 group. In contrast, C1′ in **dA2**(sg) was pyramidal, as illustrated by the N9−C1′−C2′−O dihedral angle (Scheme S2, Supporting Information). Neutral **dA2**(sg) can be alternatively described as a singlet diradical or a zwitterion. Based on the geometric features and the very different structure of the triplet diradical **dA2**(tp) (Scheme S2), we prefer to view **dA2**(sg) as a zwitterion consisting of the N1-protonated adenine ring and a C1′-carbanion. This interpretation was corroborated by the difference between the atomic charges at C1′ in **dA2**(sg) and **dA2**(tp), 0.27 and 0.54, respectively, indicating accumulation of electron density at C1′ in the singlet state. The singlet form of the N3-protonated isomer **dA3**(sg) also retained some structural features of its cation-radical precursor (**dA3**$^{+\cdot}$), namely, the strong hydrogen bond of N3-H to O5′, and pyramidal C1′ (Scheme S3). These indicated a zwitterionic character with an N3-protonated adenine ring and a C1′-carbanion. Consistent with this interpretation, the C1′ atom in **dA3**(sg) gained −0.50 units of atomic charge compared to the same atom in **dA3**(tp). The singlet state of reduced **dA4**$^{+\cdot}$ (**dA4**(sg)) had a substantially puckered purine ring and pyramidal C1′ that resembled the same features of the triplet state ((**dA4**(tp), Scheme S4). Based on these characteristics, we tentatively assigned **dA4**(sg) to be a diradical with opposite electron spins in the adenine ring and at C1′.

The $|RE_{ad}|$ of **dA2**$^{+\cdot}$-**dA4**$^{+\cdot}$ can be compared with the recombination energies of analogous protonated adenine tautomers Ad-N1-H^{+}, Ad-N-3H^{+}, and Ad-N7-H^{+} that upon reduction formed radicals Ad-N1-H$^{\cdot}$, Ad-N-3H$^{\cdot}$, and Ad-N7-H$^{\cdot}$, respectively (Scheme S5, Table S4, Supporting Information). Radical Ad-N1-H$^{\cdot}$, in which the unpaired electron is in the ring π-orbital, had a rotated NH_2 group resembling that in **dA2**(tp) but dissimilar with the structure of **dA2**(sg). Likewise, radical Ad-N3-H$^{\cdot}$ had an out-of-plane N3-H bond similar to that in **dA3**(tp), which did not occur in **dA3**(sg). Radical Ad-N7-H$^{\cdot}$ acquired a puckered imidazole ring upon reduction, which was similar to those in **dA4**(sg) and **dA4**(tp). The corresponding $|RE_{ad}|$ of adenine cations were 0.14−0.16 eV higher than those of **dA2**$^{+\cdot}$-**dA4**$^{+\cdot}$ (Table S4). This indicated that there was only a weak interaction between the π orbitals at C1′ and the purine ring. The dissimilarity of Ad-N1-H$^{\cdot}$ and Ad-N-3H$^{\cdot}$ structures relative to those of **dA2** and **dA3** was consistent with our conclusion that these noncanonical neutral adenosine molecules can be viewed as zwitterions rather than diradicals.

Electron recombination with guanosine cation-radical tautomers **dG1**$^{+\cdot}$-**dG6**$^{+\cdot}$ was associated with $|RE_{ad}|$ ranging from 7.30 to 7.62 eV (Table 5). The lowest-energy classical tautomers **dG1**$^{+\cdot}$-**dG3**$^{+\cdot}$ had $|RE_{ad}|$ of 7.46−7.54 eV. These are slightly higher than the adiabatic ionization energy reported by Pluhařová et al.[19] for **dG1** (7.41 eV) whose gas-phase structure was not conformationally optimized. The noncanonical isomers **dG7**$^{+\cdot}$-**dG9**$^{+\cdot}$ showed substantially lower recombination energies, with a low value of 4.66 eV for the global energy minimum **dG7**$^{+\cdot}$. The substantial drop of the recombination energies for the noncanonical guanosine cation-radical isomers was chiefly caused by the high relative energies of the neutral nucleosides (191−308 kJ mol^{-1} relative to **G1**, Table S5). For example, the data in Table S5 (Supporting Information) showed that the neutral singlet **dG7(sg)** from neutralization of the global energy minimum cation radical **dG7**$^{+\cdot}$ was destabilized against **dG1** by 257 kJ mol^{-1}, which largely accounted for the 2.8 eV (270 kJ mol^{-1}) difference in the ion recombination energies. The electron density distribution in **dG7(sg)** pointed to a zwitterionic structure. This was

https://doi.org/10.1021/acs.jpca.2c00894
J. Phys. Chem. A 2022, 126, 2480−2497

Scheme 2. Energetics of Proton Transfer from Noncanonical Nucleoside Cation Radicals to Nucleosides Based on CCSD(T)/CBS Single-Point Energy Calculations

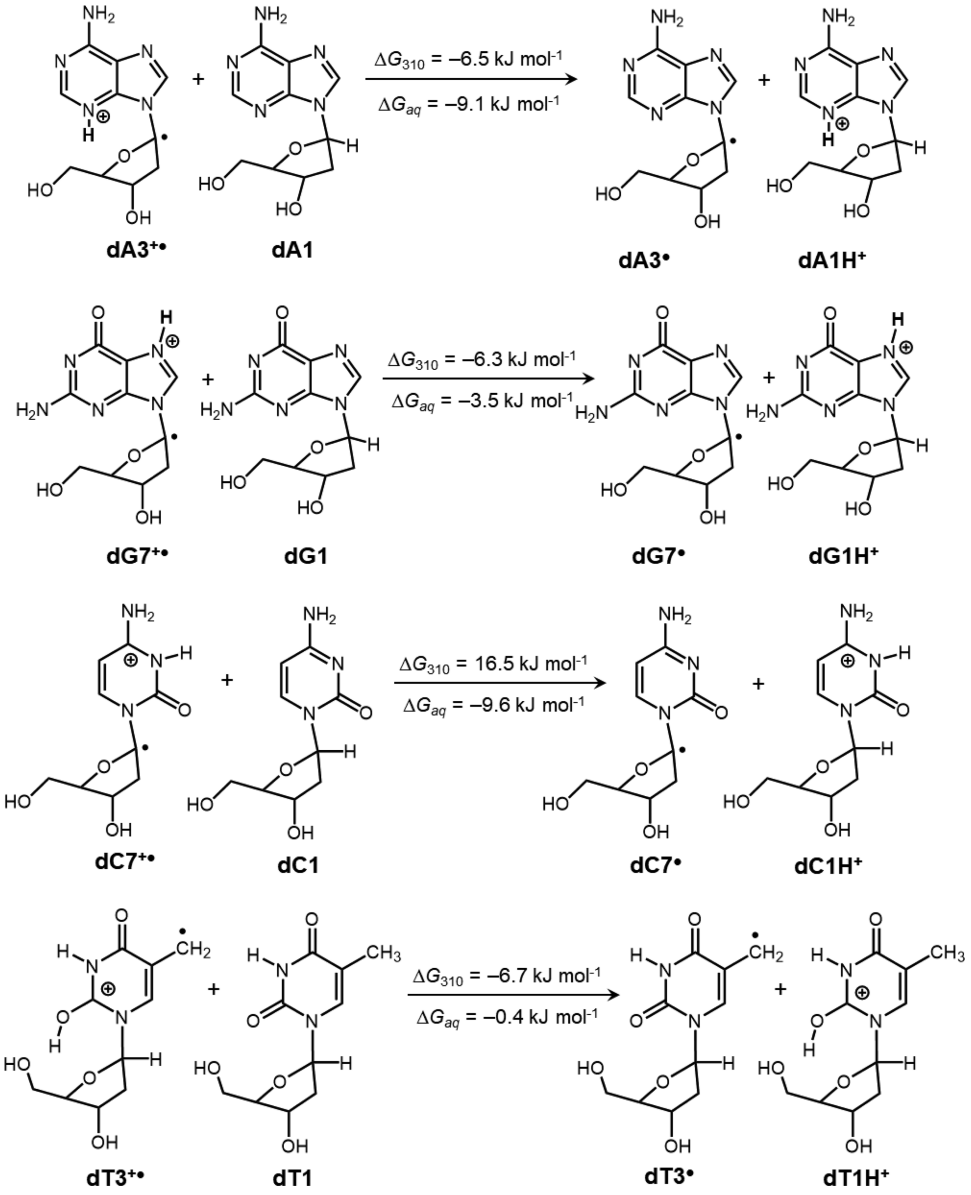

indicated by the highest occupied molecular orbital (HOMO) that had a large amplitude at C1′ and its atomic charge (0.18) compared to that in the triplet state (0.54) showing an electron flow to C1′ in the singlet state.

Adiabatic recombination energies were calculated for the canonical 2′-deoxycytidine cation radical **dC1**$^{+\bullet}$ and its substantially more stable noncanonical isomers **dC7**$^{+\bullet}$-**dC9**$^{+\bullet}$ (Table 5). The canonical $|RE_{ad}|$ = 8.14 eV was slightly higher than the DFT value for the adiabatic ionization energy reported previously.[19] The noncanonical isomers showed much lower $|RE_{ad}|$ that ranked within 4.93−5.12 eV. Electron recombination with the planar isomer **dC7**$^{+\bullet}$ produced a singlet neutral (**dC7(sg)**) that retained the coplanar arrangement of the cytosine and ribose rings. This resulted in a delocalization of the HOMO over C1′ and the cytosine π-electron system (Scheme S6, Supporting Information). Electron recombination with the C1′-pyramidized isomer **dC8**$^{+\bullet}$ formed a neutral singlet (**dC8(sg)**) which also retained a pyramidized structure, giving a HOMO that had a large amplitude at C1′ (Scheme S7, Supporting Information).

Electron recombination with noncanonical thymidine cation radicals gave neutral singlet molecules depending on the initial radical site. With **dT3**$^{+\bullet}$ having a C5 exocyclic methylene group, the neutral singlet **dT3(sg)** that was formed at $|RE_{ad}|$ = 5.24 eV (Table 5) can be represented as a polarized zwitterion with a negative charge at the 5-methylene and a positive charge at C2 (Scheme S8, Supporting Information). For the low-energy C1′ radical **dT7**$^{+\bullet}$, electron recombination resulted in a singlet structure with coplanar rings, **dT7(sg)**, and $|RE_{ad}|$ = 4.95 eV. The atomic electron densities again pointed to a zwitterionic structure with positively charged C1′ and negative charge at C5 and C6 (Scheme S8). The canonical thymidine isomer **dT1**$^{+\bullet}$ had $|RE_{ad}|$ = 8.20 eV, consistent with the previously reported DFT ionization energy of neutral thymidine.[19]

The $|RE_{ad}|$ data for the lowest-energy noncanonical isomers of the nucleoside cation radicals point to a substantially

https://doi.org/10.1021/acs.jpca.2c00894
J. Phys. Chem. A 2022, 126, 2480−2497

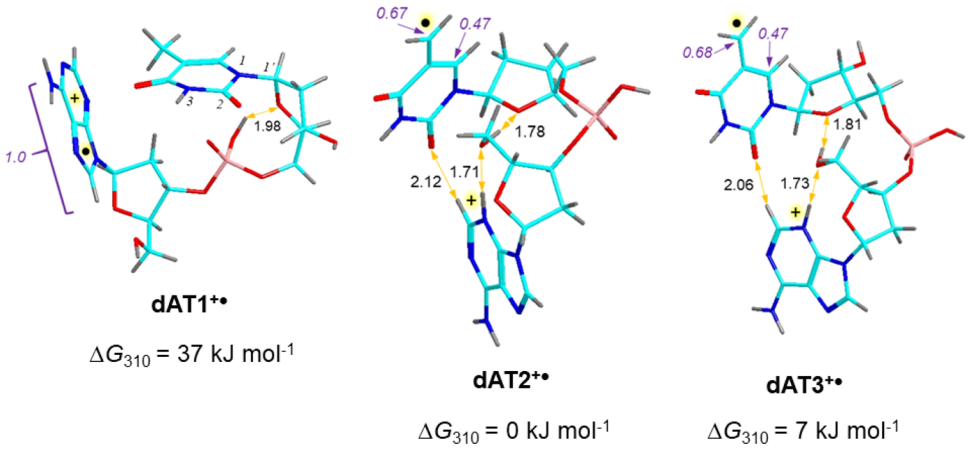

Figure 5. M06-2X/6−31 + G(d,p)-optimized structures of low-energy $dAT^{+\cdot}$ nucleotide cation radicals. Yellow double-headed arrows indicate hydrogen bonds with distances in Ångstrøms. Purple italics represent NPA atomic spin densities. Relative Gibbs energies are from M06-2X/6−311++G(2d,p) calculations with B3LYP/6−31 + G(d,p) zero-point energies, enthalpies, and entropies.

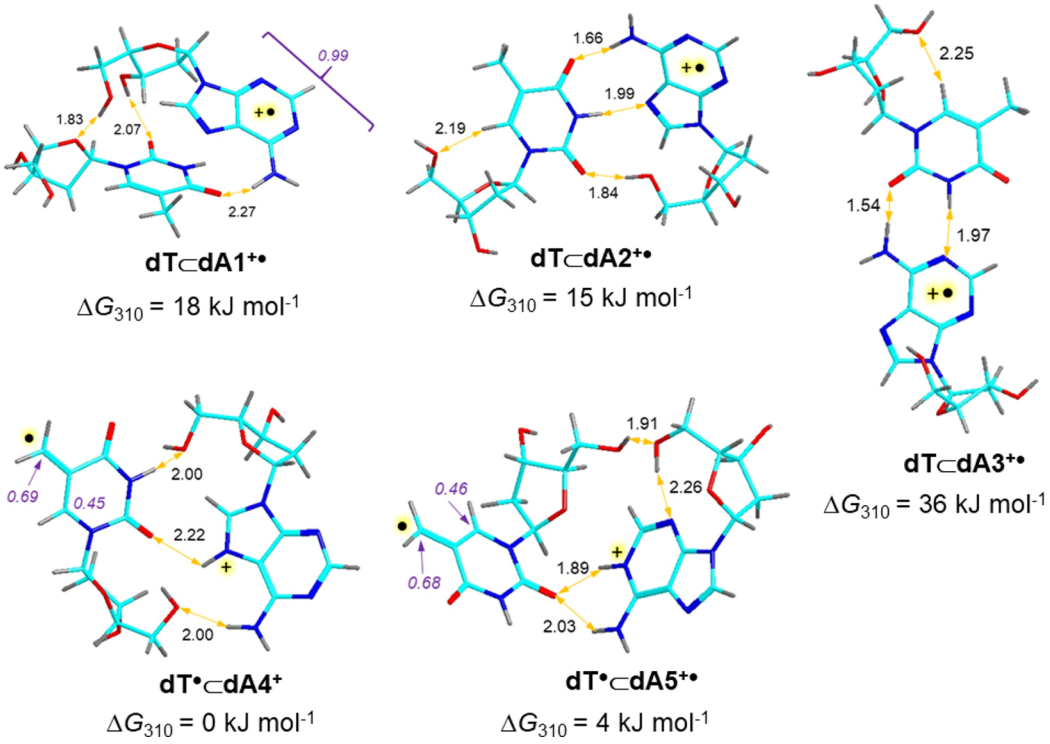

Figure 6. M06-2X/6−31 + G(d,p)-optimized structures of low-energy $dTdA^{+\cdot}$ cation radical pairs. Description as in Figure 5.

reduced oxidation potential of these ions for abstracting an electron from any of the canonical nucleobases. Thus, if any noncanonical nucleoside cation radical was formed in DNA, it could not capture an electron from a canonical nucleobase. The $|RE_{ad}|$ ranking among the noncanonical nucleoside cation radicals followed the sequence $|RE_{ad}|(\mathbf{dC7}^{+\cdot}) > |RE_{ad}|(\mathbf{dT7}^{+\cdot}) > |RE_{ad}|(\mathbf{dA3}^{+\cdot}) > |RE_{ad}|(\mathbf{dG7}^{+\cdot})$ which was not unlike an analogous sequence for the canonical forms, $|RE_{ad}|(\mathbf{dT1}^{+\cdot}) > |RE_{ad}|(\mathbf{dC1}^{+\cdot}) > |RE_{ad}|(\mathbf{dA1}^{+\cdot}) > |RE_{ad}|(\mathbf{dG1}^{+\cdot})$, with the $|RE_{ad}|$ for $\mathbf{dC7}^{+\cdot}$ and $\mathbf{dT7}^{+\cdot}$ reversed.

Cation Radicals of Dinucleotides and Nucleoside Pairs. Whereas the noncanonical nucleoside cation radicals have extremely low recombination energies, preventing them from abstracting an electron from canonical nucleobases, they may undergo other reactions, such as proton transfer between nucleosides in the same DNA strand or in Watson−Crick pairs. We investigated the energetics of proton transfer between separate noncanonical nucleoside cation radicals and canonical neutral nucleosides, as well as the proton transfer dynamics in combinations of ionized dinucleotides $dAT^{+\cdot}$ and $dCT^{+\cdot}$ and noncovalent $dA{\subset}dT^{+\cdot}$ Watson−Crick complexes. Gas-phase energies for the nucleosides were obtained from single-point CCSD(T)/CBS calculations, and solvation energies were from geometry optimizations with PCM-M06-2X/6−311++G(2d,p).

Proton transfer from the lowest-energy adenosine cation radical $\mathbf{dA3}^{+\cdot}$ to neutral adenine (**dA1**) was calculated to be mildly exergonic ($\Delta G_{310} = -6.5$ kJ mol^{-1}) in the gas phase, forming radical $\mathbf{dA3}^{\bullet}$ along with the lowest-energy protonated adenosine $\mathbf{dA1H}^{+}$ (Scheme 2). Solvation with water had only a

https://doi.org/10.1021/acs.jpca.2c00894
J. Phys. Chem. A 2022, 126, 2480−2497

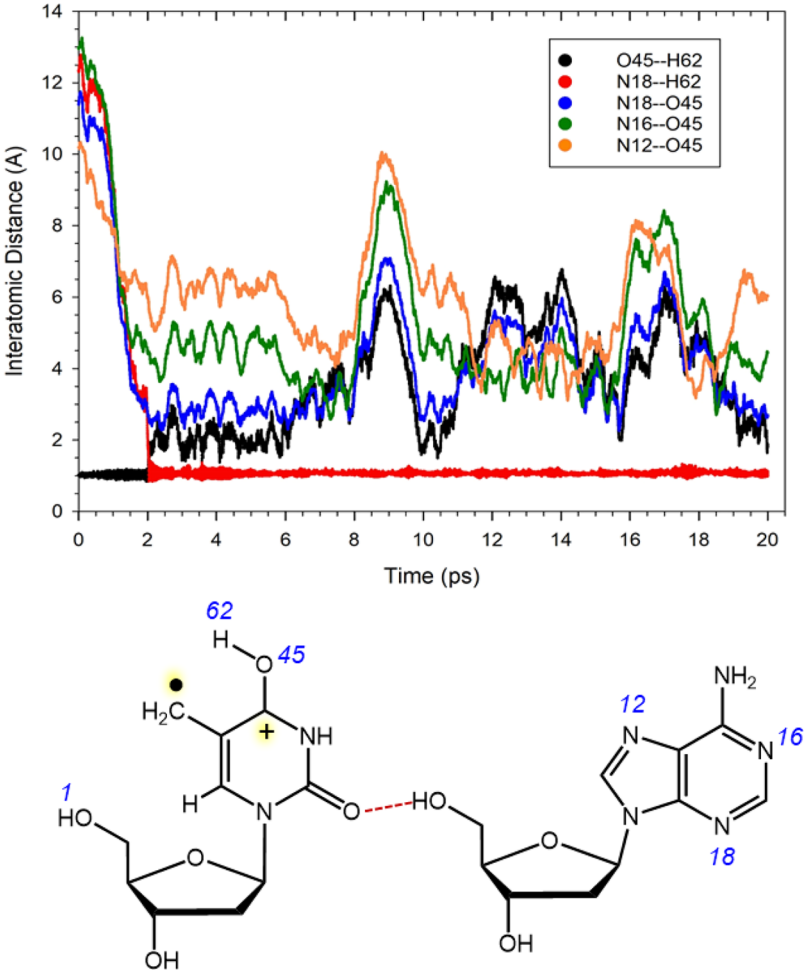

Figure 7. Top panel: Plot of selected interatomic distances in the $\mathbf{dT^{+\cdot}{\subset}dA}$ pair in the course of a 20 ps BOMD trajectory. For atom numbering, see the bottom panel.

small effect on the proton transfer thermochemistry, increasing the reaction exergonicity to −9.1 kJ mol^{-1}. Proton transfer from the lowest-energy guanosine cation radical $\mathbf{dG7^{+\cdot}}$ to neutral guanine (**dG1**) was also mildly exergonic both in the gas phase (ΔG_{310} = −1.9 kJ mol^{-1}, Scheme 2) and when including solvation with water (ΔG_{310} = −3.5 kJ mol^{-1}).

Proton transfer to cytidine **dC1** from the lowest-energy cytidine cation radical $\mathbf{dC7^{+\cdot}}$ was 16.5 kJ mol^{-1} endergonic in the gas phase. This was reversed by solvation in water dielectric making the proton transfer between solvated cytidine nucleosides 9.6 kJ mol^{-1} exergonic. Finally, proton transfer to neutral thymidine **dT1** from the lowest-energy noncanonical cation radical $\mathbf{dT3^{+\cdot}}$ was mildly exergonic in the gas phase (ΔG_{310} = −6.7 kJ mol^{-1}) to become nearly thermoneutral (ΔG_{310} = −0.4 kJ mol^{-1}) for the solvated ions. These Gibbs energies showed that the presence of the C1′ radical in $\mathbf{dA3^{+\cdot}}$, $\mathbf{dG7^{+\cdot}}$ and $\mathbf{dC7^{+\cdot}}$, as well as the C5-methyl radical in $\mathbf{dT3^{+\cdot}}$, had only a small effect on the nucleobase basicity.

$\mathbf{dAT^{+\cdot}}$ Dinucleotides and Ion Pairs. Geometry optimization of $dAT^{+\cdot}$ dinucleotides consisting of neutral adenosine and noncanonical thymine cation radicals resulted in a spontaneous proton transfer from the thymine ion to adenine, cf. structures $\mathbf{dAT2^{+\cdot}}$ and $\mathbf{dAT3^{+\cdot}}$ (Figure 5). These are distonic ions with separated radical and charge sites in which the unpaired electron is at the thymine C5 methylene and C6 positions, whereas the charge is on the adenine. In contrast, a $dAT^{+\cdot}$ dinucleotide consisting of canonical adenine and thymine nucleosides produced upon geometry optimization a canonical adenine-ionized cation radical $\mathbf{dAT1^{+\cdot}}$ which had a 37 kJ mol^{-1} higher energy than $\mathbf{dAT2^{+\cdot}}$. Similar results were obtained for geometry optimizations of ionized adenosine-thymidine pairs (Figure 6).

The low-energy canonical forms of $\mathbf{dT{\subset}dA1^{+\cdot}}$-$\mathbf{dT{\subset}dA3^{+\cdot}}$ consisted of an adenosine cation radical and neutral thymine but did not isomerize by proton transfer. This was regardless of the initial nucleoside orientation and thermal motion in 100 ps BOMD trajectories at 350 K. Interestingly, the relative Gibbs energies of $dT{\subset}dA^{+\cdot}$ complexes did not favor Watson−Crick pairs $\mathbf{dT{\subset}dA2^{+\cdot}}$ and $\mathbf{dT{\subset}dA3^{+\cdot}}$ relative to $\mathbf{dT{\subset}dA1^{+\cdot}}$, which had a different hydrogen bonding pattern. In contrast to the canonical nucleosides, $dT^{+}{\subset}dA^{+\cdot}$ pairs in which the thymine cation radical had a noncanonical initial structure with a C5-methylene underwent spontaneous proton transfer to adenosine, forming the lowest-energy distonic ions $\mathbf{dT^{\cdot}{\subset}dA4^{+}}$ and $\mathbf{dT^{\cdot}{\subset}dA5^{+}}$.

We further pursued investigations of proton transfer by analyzing 20 ps BOMD trajectories starting from several initial complex structures that were composed of noncanonical $\mathbf{dT^{+\cdot}}$ and neutral **dA**. These yielded very similar results regardless of the initial nucleoside orientation, as illustrated with the trajectory shown in Figure 7 and the associated scheme that indicates the atom numbering. The acidic proton (H62) in

https://doi.org/10.1021/acs.jpca.2c00894
J. Phys. Chem. A 2022, 126, 2480−2497

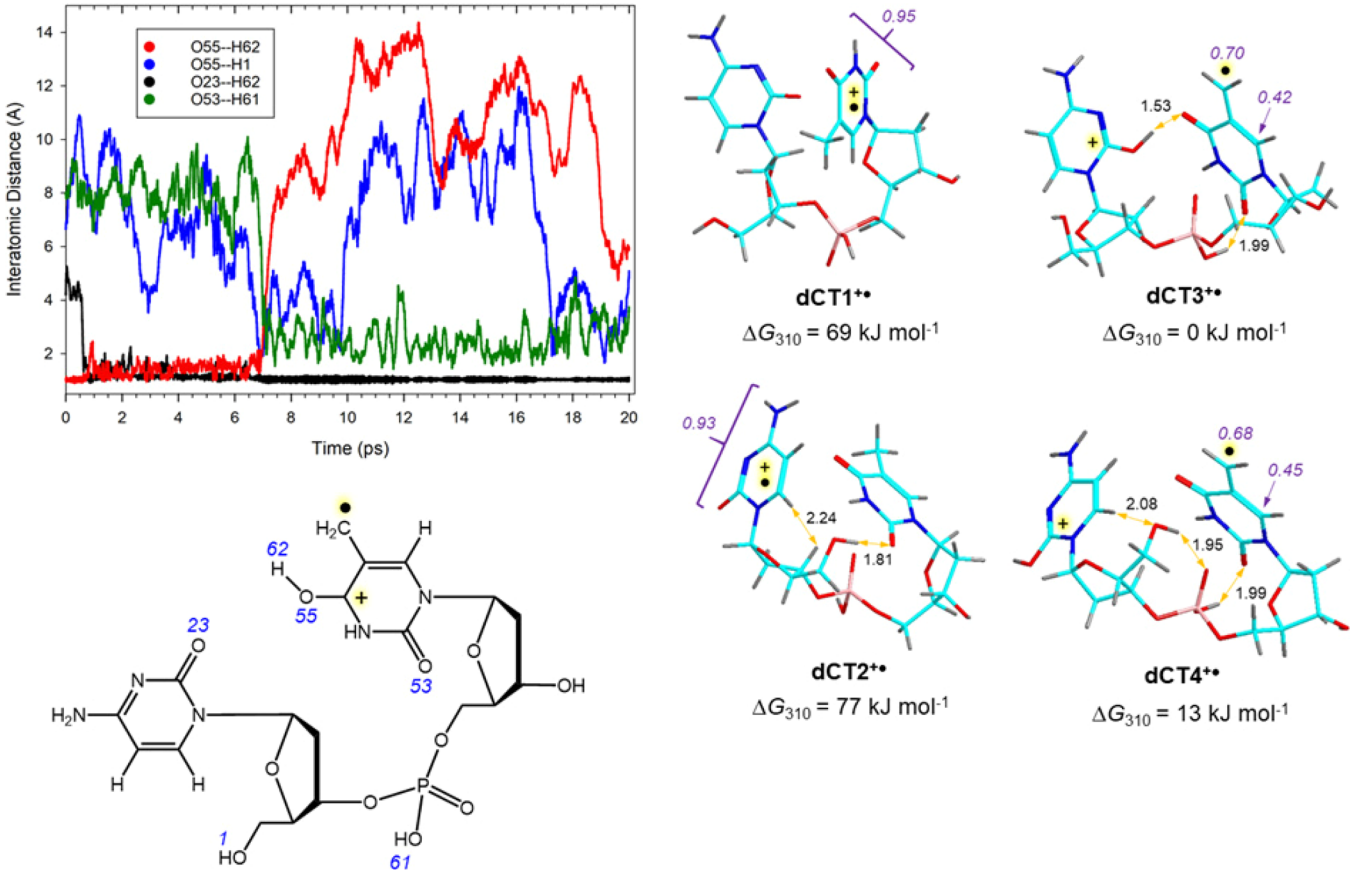

Figure 8. Left panel: Plot of selected interatomic distances in the **dCT**$^{+\cdot}$ dinucleotide cation radical in the course of a 20 ps BOMD trajectory. For atom numbering, see the bottom panel. Relative Gibbs energies are from M06-2X/6−311++G(2d,p) calculations with B3LYP/6−31 + G(d,p) zero-point energies, enthalpies, and entropies.

dT$^{+\cdot}$ was initially at O4 (atom O45 in Figure 7) at a long distance from the basic adenine nitrogens. Thermal motion at 350 K led to a rapid conformation change that brought the thymine OH close to the adenine N3 (atom N18 in Figure 7) within 2 ps, resulting in proton transfer. The thymine oxygen (O45) remained hydrogen bonded to adenine H62−N18, but this interaction was periodically disrupted by thermal motion, as evidenced by the oscillating O45−H62 distance (Figure 7). Interestingly, we did not observe thymine proton transfer to adenine N1 (atom N16 in Figure 7) or N7 (atom N12 in Figure 7) which are the less basic sites in adenosine. However, transfer to those adenine positions may occur if many more (>100) trajectories were run.

The energetics of thymine-containing dinucleotide cation radicals and complexes indicated thermodynamically favorable and very fast isomerizations involving a hydroxyl hydrogen migration from the noncanonical thymine cation radical. The resulting thymine C5-methylene radicals, for example, **dT**$^{\cdot}$**⊂dA4**$^{+}$ and **dT**$^{\cdot}$**⊂dA5**$^{+}$, were analogous to the intermediates of methyl hydrogen abstraction from ionized canonical thymine, as studied in solution by Schuster and co-workers.[10−14] The formation of thymine radicals has been attributed to fast proton transfer to water. The present data indicate an alternative mechanism for the thymine-centered radical formation, involving noncanonical cation radical isomers as highly reactive intermediates. Thus, noncanonical nucleotide cation radicals can be viewed as a hitherto unrecognized dark matter of DNA ionization that can explain some aspects of reactions following the cation-radical formation.

dCT$^{+\cdot}$ **and dTC**$^{+\cdot}$ **Dinucleotides.** To further examine if the adenine-thymine interaction was unique, we analyzed 20 ps trajectories of dCT$^{+\cdot}$ dinucleotides containing an initial noncanonical thymine cation radical. The initial structure shown in Figure 8 had the thymine OH (atom numbers O55 and H62 in Figure 8) at >4 Å from the cytosine O2 (atom number O23 in Figure 8). Upon thermal motion at 350 K, the dinucleotide conformation underwent a rapid collapse, bringing H62 to O23 at ca. 0.8 ps, while maintaining a strong O55−H62−O23 hydrogen bond for additional 6 ps. This hydrogen bond was disrupted at 7 ps by a temporary formation of new hydrogen bonds between O55 and the 5′ hydroxyl (H1) and the thymine O2 and phosphoester OH (atom numbers O53 and H61, respectively). These hydrogen bonds showed periodic disruption and reformation in the course of the 20 ps trajectory. Overall, proton transfer from the noncanonical thymine ion to cytosine was highly exergonic. This is shown by the Gibbs energies of canonical **dCT1**$^{+\cdot}$ and **dCT2**$^{+\cdot}$ ions that were ionized in cytosine, according to the canonical nucleobase recombination energies, relative to **dCT3**$^{+\cdot}$ and **dCT4**$^{+\cdot}$ that underwent a thymine-to-cytosine proton transfer (Figure 8).

Very similar results were obtained by running and analyzing BOMD trajectories for dTC$^{+\cdot}$ dinucleotides. The representative Figure 9 trajectory showed a rapid transfer of the hydroxyl proton from the thymine cation radical to O5′ which was followed by a conformational collapse bringing the cytosine O2 close to the 5′-OH2 group and resulting in proton transfer. Overall, the isomerization by proton transfer from the noncanonical cation radical **dTC1**$^{+\cdot}$ to the cytosine-protonated

https://doi.org/10.1021/acs.jpca.2c00894
J. Phys. Chem. A 2022, 126, 2480−2497

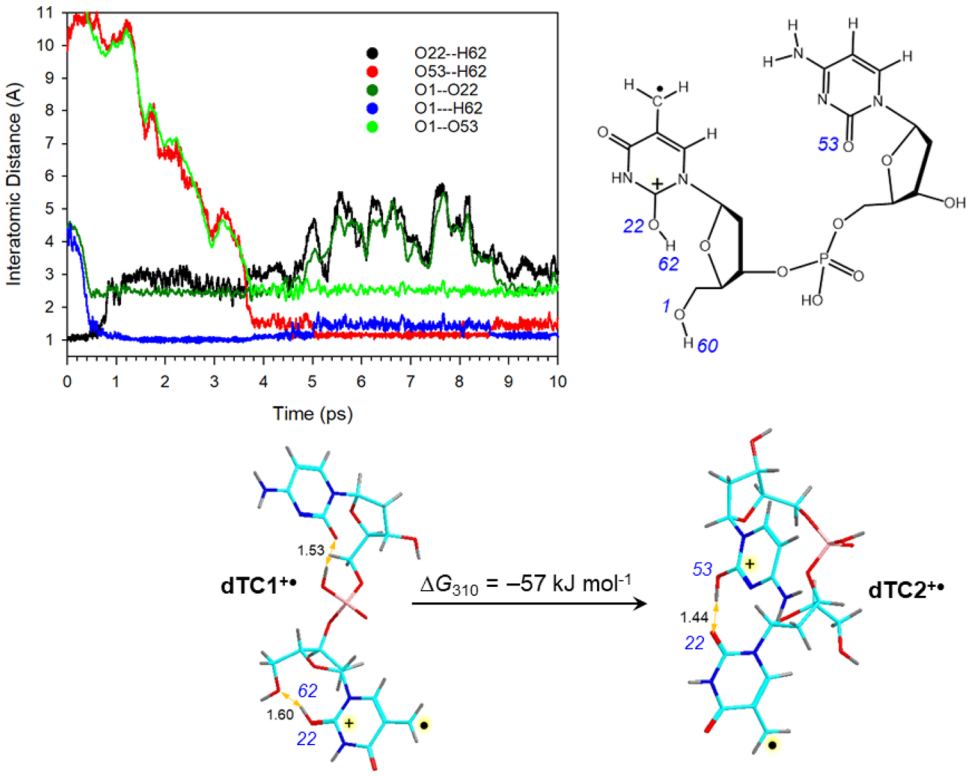

Figure 9. Left panel: Plot of selected interatomic distances in the **dTC**$^{+\bullet}$ dinucleotide cation radical in the course of a 20 ps BOMD trajectory. No significant changes in interatomic distances were observed after 10 ps. For atom numbering, see the right panel. Relative Gibbs energies are from M06-2X/6−311++G(2d,p) calculations with B3LYP/6−31 + G(d,p) zero-point energies, enthalpies, and entropies.

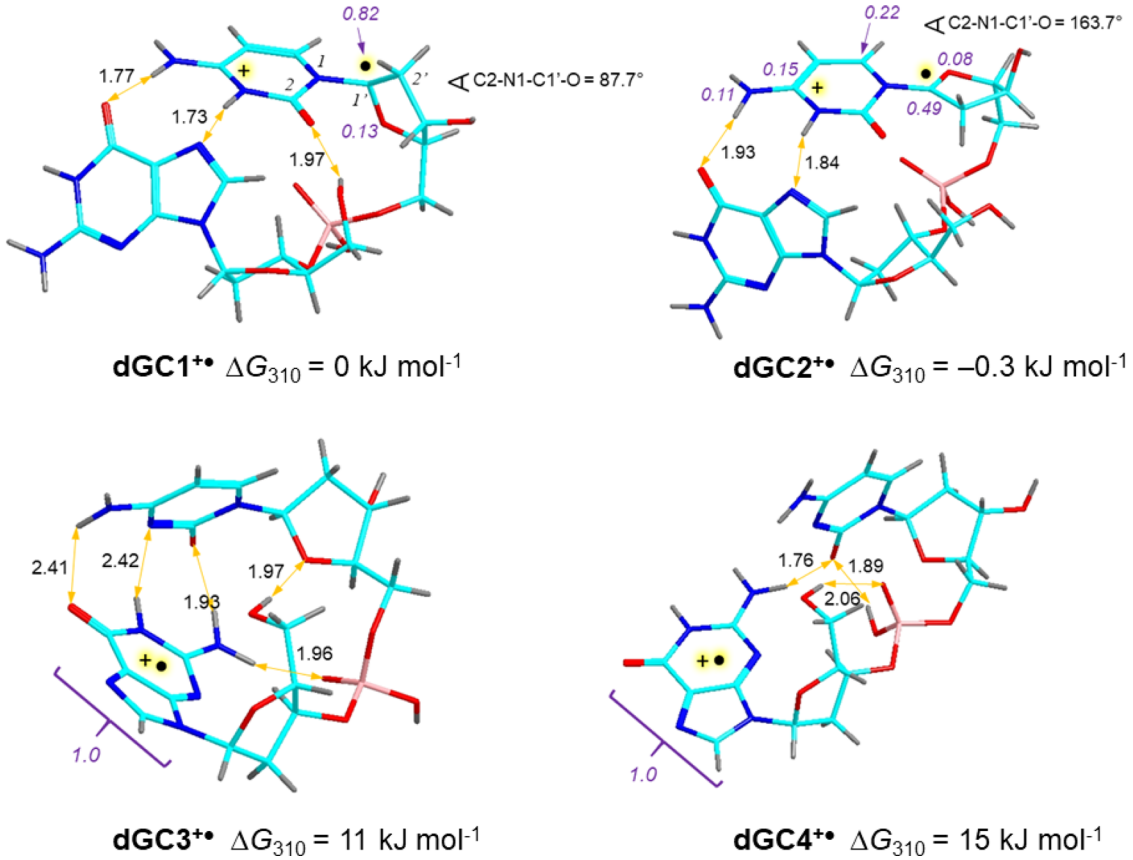

Figure 10. M06-2X/6−31 + G(d,p)-optimized structures of low-energy dGC$^{+\bullet}$ dinucleotide cation radicals. Description as in Figure 5.

https://doi.org/10.1021/acs.jpca.2c00894
J. Phys. Chem. A 2022, 126, 2480−2497

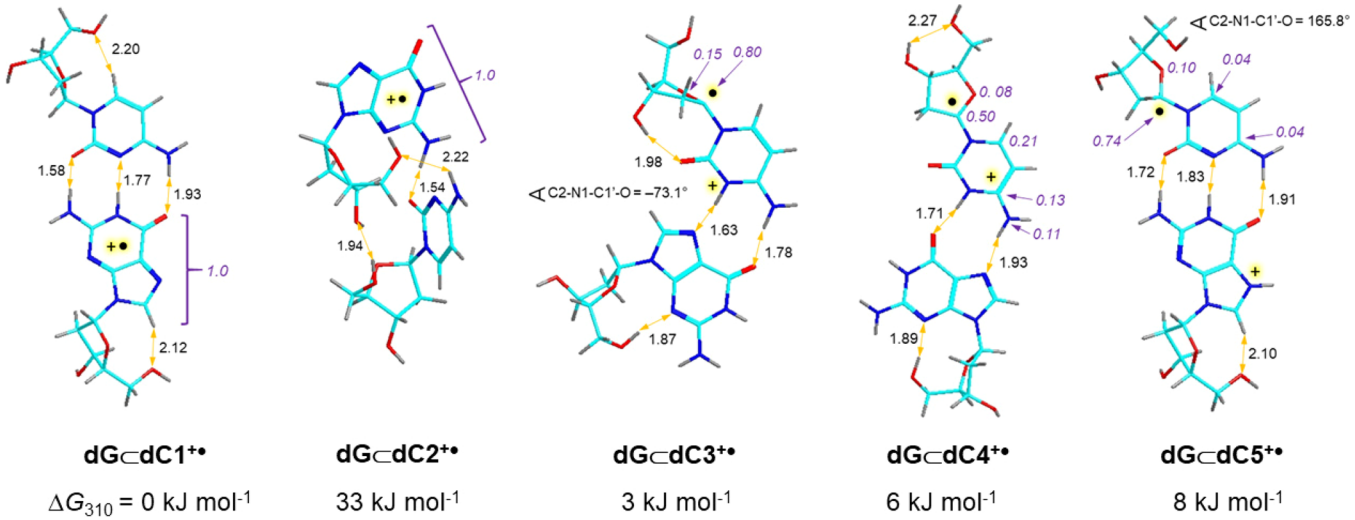

Figure 11. M06-2X/6−31 + G(d,p)-optimized structures of low-energy $dGC^{+\cdot}$ dinucleotide cation radicals. Description as in Figure 5.

thymine radical **dTC2**$^{+\cdot}$ was 57 kJ mol^{-1} exergonic, as established for low-energy fully optimized conformers, providing the driving force for the reaction (Figure 9).

dGC$^{+\cdot}$ Dinucleotides and Ion Pairs. Interactions between ionized cytidine and guanosine were investigated in dinucleotides **dGC1**$^{+\cdot}$-**dGC4**$^{+\cdot}$ and nucleoside pairs **dG⊂dC1**$^{+\cdot}$-**dG⊂dC5**$^{+\cdot}$. These represent the lowest Gibbs energy structures from each type of ion. The two low-energy dinucleotide structures with noncanonical cytidine units, **dGC1**$^{+\cdot}$ and **dGC2**$^{+\cdot}$, were both protonated at cytosine N-3 and nearly isoenergetic, but differed in their electronic structure. Ion **dGC1**$^{+\cdot}$ had a pyramidal arrangement at C1′ that carried most of spin density, whereas the guanine ring was neutral. In contrast, ion **dGC2**$^{+\cdot}$ had a coplanar arrangement of the cytosine and 2′-deoxyribose rings, which resulted in spin density delocalization into the cytosine π-electron system (Figure 10). These two ions illustrate the stability of the noncanonical cytidine cation-radical moiety even in a dinucleotide ion where it is engaged in close-range hydrogen bonding to guanine. Two low-energy canonical isomers were obtained (**dGC3**$^{+\cdot}$ and **dGC4**$^{+\cdot}$) that were ionized in guanosine, as evidenced by the complete retention of spin density in the guanine ring. Ions **dGC3**$^{+\cdot}$ and **dGC4**$^{+\cdot}$ had similar relative Gibbs energies that were higher than those of **dGC1**$^{+\cdot}$ and **dGC2**$^{+\cdot}$. Interestingly, there was only a very small energy preference for the Watson−Crick nucleobase arrangement in **dGC3**$^{+\cdot}$ compared to the different ring orientation in the other conformer **dGC4**$^{+\cdot}$. The latter ion gained stabilization by forming additional hydrogen bonds to the 5′ and phosphate hydroxyls. Also noteworthy is the substantial weakening of the hydrogen bonds between guanine and cytosine in ion **dGC3**$^{+\cdot}$ as a result of guanine ionization. The indicated thermodynamic stability of the noncanonical GC dinucleotide cation radicals indicated that if formed by ionization, the GC unit in DNA would not isomerize to ionized guanine, thus preventing hole migration.

Among the several **dG⊂dC**$^{+\cdot}$ dinucleoside pairs we investigated, the Watson−Crick pair **dG⊂dC1**$^{+\cdot}$ was only marginally more stable than structures consisting of neutral guanosine and noncanonical ionized cytidine, **dG⊂dC3**$^{+\cdot}$ through **dG⊂dC5**$^{+\cdot}$ (Figure 11). Ion **dG⊂dC1**$^{+\cdot}$ was ionized in guanine, as evidenced by the complete spin density retention in the guanine ring. Molecular orbital analysis with M06-2X/6−311++G(2d,p) of **dG⊂dC1**$^{+\cdot}$ showed delocalization of the top occupied alpha orbitals, MO130α and MO129α, in the guanine and cytosine π-electron systems, whereas the highest energy occupied β orbital (MO129β) was on cytidine (Figure S1, Supporting Information). This differed from the previous report on the ionized Watson−Crick guanine-cytosine pair by Kumar and Sevilla who assigned the HOMO to be on cytosine.[80] Our analysis showed that the energy spacing of the frontier alpha and beta orbitals in **dG⊂dC1**$^{+\cdot}$ was quite tight (within 0.14 eV) and could be possibly reversed depending on the ion system and computational method used. This dependence on the ion geometry is illustrated by the analysis of frontier orbitals in **dG⊂dC2**$^{+\cdot}$, **dGC3**$^{+\cdot}$, and **dGC4**$^{+\cdot}$. Ion **dG⊂dC2**$^{+\cdot}$ showed the HOMO (MO130α) to be a cytosine π-orbital with the underlying MO129α being a guanine π-orbital. The energy difference between MO130α and MO129α was only 0.04 eV (Figure S2, Supporting Information). Similarly, the canonical dinucleotide ion structures **dGC3**$^{+\cdot}$ and **dGC4**$^{+\cdot}$ showed a different order of frontier MOs, with the former ion having the guanine π-orbital (MO 145α) at the highest energy (Figure S3, Supporting Information). This was reversed in **dGC4**$^{+\cdot}$ where the cytosine π-orbital (MO 145α) was 0.05 eV higher than the guanine π-orbital (MO144α) (Figure S4, Supporting Information). We note that spin-unrestricted M06-2X calculations have been found to provide accurate excitation energies for cation radicals of several canonical and noncanonical nucleobases,[38,39,74,81,82] nucleosides,[83,84] and nucleotides,[85−89] as determined by comparison with both experimental UV−vis action spectra and benchmarking on equation-of-motion coupled cluster calculations.

Ion **dG⊂dC1**$^{+\cdot}$ displayed three strong hydrogen bonds linking the nucleobases. The alternative canonical pair **dG⊂dC2**$^{+\cdot}$ which had hydrogen bonds between neutral cytosine and the 2′-deoxyribose hydroxyls was substantially less stable than **dG⊂dC1**$^{+\cdot}$. The noncanonical isomers retained the cytidine cation-radical structure, with protonation at cytosine N-3 and a C1′ radical site. In contrast to the **dT⊂dA**$^{+\cdot}$ pairs, there was no propensity among the noncanonical **dG⊂dC**$^{+\cdot}$ to undergo proton transfer to guanine. Conversely, BOMD trajectories originating from structures

https://doi.org/10.1021/acs.jpca.2c00894
J. Phys. Chem. A 2022, 126, 2480−2497

protonated at guanine N7 showed a very rapid proton transfer to N3 of the cytosine ring, such as in **dG⊂dC3**$^{+\bullet}$. A distonic arrangement of the radical and charge sites residing in different nucleobases was found in low-energy structure **dG⊂dC5**$^{+\bullet}$ which was at 8 kJ mol^{-1} relative to **dG⊂dC1**$^{+\bullet}$ and had a Watson−Crick hydrogen bonding between the nucleobases (Figure 11). The stability of **dG⊂dC3**$^{+\bullet}$ was consistent with the calculated proton affinities of the **dC3** radical (PA = 1008 kJ mol^{-1}) and guanosine (993 kJ mol^{-1}) that indicated that proton transfer to guanine would be endergonic.

The calculated structures and energetics of the **dG⊂dC**$^{+\bullet}$ pairs indicated that the complexes were stable structures corresponding to local energy minima. This was consistent with the results of a previous study by O′Hair and co-workers who reported a stable **dG⊂dC**$^{+\bullet}$ cation radical complex that was generated by gas-phase dissociation of a Cu^{II} complex.[90] As a minor difference from O′Hair and co-workers,[90] we found, via a thorough conformational analysis, a low-energy non-Watson−Crick canonical isomer **dG⊂dC2**$^{+\bullet}$, in addition to the noncanonical structures **dG⊂dC3**$^{+\bullet}$-**dG⊂dC5**$^{+\bullet}$ (Figure 11).

CONCLUSIONS

Ab initio calculations at a high level of theory and in combination with BOMD analysis of ion conformations reveal a new class of thermodynamically stable nucleosides, nucleoside pairs, and dinucleotide cation radicals. These new noncanonical cation radicals have separated charge and radical sites resulting from the migration of a deoxyribose hydrogen atom from C1′ to a basic position in the nucleobase. DNA components of this type have rarely been considered in the current models of DNA radiation damage nor have they been sought in experimental and computational studies. We therefore call these new species the dark matter of DNA ionization. Our computational analysis further reveals that noncanonical cation radicals of nucleosides, dinucleotides, and nucleoside pairs have a distinct electronic structure that fundamentally differs from that in canonical ions. The low energies of the cation radicals, combined with the high energies of their corresponding neutral species, converge to extremely low recombination energies of the noncanonical cation radicals making them deep hole traps incapable of extracting an electron from canonical nucleosides. Noncanonical dA$^{+\bullet}$ and dG$^{+\bullet}$ were calculated to be relatively weak acids when compared with neutral nucleosides. In contrast, noncanonical dT$^{+\bullet}$ can undergo exothermic and fast (ps) proton transfer to dA and dC, forming a thymine radical that can play a role in downstream chemical reactions.

ASSOCIATED CONTENT

Supporting Information

The Supporting Information is available free of charge at https://pubs.acs.org/doi/10.1021/acs.jpca.2c00894.

Additional figures including optimized structures, reaction schemes, and molecular orbital analysis; tables of calculated relative energies (PDF)

AUTHOR INFORMATION

Corresponding Author

František Tureček − *Department of Chemistry, University of Washington, Seattle, Washington 98195-1700, United States;* orcid.org/0000-0001-7321-7858; Phone: +1-206-685-2041; Email: turecek@uw.edu

Author

Shu R. Huang − *Department of Chemistry, University of Washington, Seattle, Washington 98195-1700, United States*

Complete contact information is available at: https://pubs.acs.org/10.1021/acs.jpca.2c00894

Notes

The authors declare no competing financial interest.

ACKNOWLEDGMENTS

Support from the Chemistry Division of the U.S. National Science Foundation (Grant CHE-1951518) and the Klaus and Mary Ann Saegebarth Endowment is gratefully acknowledged.

REFERENCES

(1) Mohler, S. R. Galactic Radiation Exposure during Commercial Flights: Is There a Risk? *Can. Med. Assoc. J.* **2003**, *168*, 1157−1158.
(2) Lehnert, S. *Biomolecular Action of Ionizing Radiation*; CRC Press: Boca Raton, FL, 2007.
(3) Desouky, O.; Ding, N.; Zhou, G. Targeted and Non-Targeted Effects of Ionizing Radiation. *J. Rad. Res. Appl. Sci.* **2015**, *8*, 247−254.
(4) Wagenknecht, H.-A., Ed.; *Charge Transfer in DNA*; Wiley-VCH, Weinhem, Germany; 2005.
(5) Douki, T.; Ravanat, J.-L.; Angelov, D.; Wagner, J. R.; Cadet, J. Effects of Duplex Stability on Charge-Transfer Efficiency within DNA. *Top. Curr. Chem.* **2004**, *236*, 1−25.
(6) Kawai, K.; Majima, T. Hole Transfer Kinetics of DNA. *Acc. Chem. Res.* **2013**, *46*, 2616−2625.
(7) Genereux, J. C.; Boal, A. K.; Barton, J. K. DNA-Mediated Charge Transport in Redox Sensing and Signaling. *J. Am. Chem. Soc.* **2010**, *132*, 891−905.
(8) Giese, B. Long-Distance Charge Transport in DNA: The Hopping Mechanism. *Acc. Chem. Res.* **2000**, *33*, 631−636.
(9) Giese, B. Long-Distance Electron Transfer Through DNA. *Annu. Rev. Biochem.* **2002**, *71*, 51−70.
(10) Joy, A.; Ghosh, A. K.; Schuster, G. B. One-Electron Oxidation of DNA Oligomers That Lack Guanine: Reaction and Strand Cleavage at Remote Thymines by Long-Distance Radical Cation Hopping. *J. Am. Chem. Soc.* **2006**, *128*, 5346−5347.
(11) Ghosh, A.; Joy, A.; Schuster, G. B.; Douki, T.; Cadet, J. Selective One-Electron Oxidation of Duplex DNA Oligomers: Reaction at Thymines. *Org. Biomol. Chem.* **2008**, *6*, 916−928.
(12) Joseph, J.; Schuster, G. B. Oxidatively Damaged Nucleobases in Duplex DNA Oligomers: Reaction at Thymine-Thymine Mispairs. *J. Am. Chem. Soc.* **2009**, *131*, 13904−13905.
(13) Kanvah, S.; Schuster, G. B. One-Electron Oxidation of DNA: Thymine versus Guanine Reactivity. *Org. Biomol. Chem.* **2010**, *8*, 1340−1343.
(14) Barnett, R. N.; Joseph, J.; Landman, U.; Schuster, G. B. Oxidative Thymine Mutation in DNA: Water-Wire-Mediated Proton-Coupled Electron Transfer. *J. Am. Chem. Soc.* **2013**, *135*, 3904−3914.
(15) Improta, R.; Scalmani, G.; Barone, V. Radical Cations of DNA Bases: Some Insights on Structure and Fragmentation Patterns by Density Functional Methods. *Int. J. Mass Spectrom.* **2000**, *201*, 321−336.
(16) Close, D. M.; Ehmann, K. T. Ionization Energies of the Nucleotides. *J. Phys. Chem. A* **2008**, *112*, 11207−11212.
(17) Zhou, J.; Kostko, O.; Nicolas, C.; Tang, X.; Belau, L.; de Vries, M. S.; Ahmed, M. Experimental Observation of Guanine Tautomers with VUV Photoionization. *J. Phys. Chem. A* **2009**, *113*, 4829−4832.
(18) Pluhařová, E.; Jungwirth, P.; Bradford, S. E.; Slavíček, P. Ionization of Purine Tautomers in Nucleobases, Nucleosides, and Nucleotides: From the Gas Phase to the Aqueous Environment. *J. Phys. Chem. B* **2011**, *115*, 1294−1305.

(19) Pluhařová, E.; Slavíček, P.; Jungwirth, P. Modeling Photoionization of Aqueous DNA and Its Components. *Acc. Chem. Res.* **2015**, *48*, 1209−1217.
(20) Capobianco, A.; Caruso, T.; Peluso, A. Hole Delocalization over Adenine Tracts in Single Stranded DNA Oligonucleotides. *Phys. Chem. Chem. Phys.* **2015**, *17*, 4750−4756.
(21) Kumar, A.; Pottiboyina, V.; Sevilla, M. D. One-Electron Oxidation of Neutral Sugar Radicals of 2′-Deoxyguanosine and 2′-Deoxythymidine: A Density Functional Theory (DFT) Study. *J. Phys. Chem. B* **2012**, *116*, 9409−9416.
(22) Dolgounitcheva, O.; Zakrzewski, V. G.; Ortiz, J. V. Ionization Energies and Dyson Orbitals of Cytosine and 1-Methylcytosine. *J. Phys. Chem. A* **2003**, *107*, 822−828.
(23) Roca-Sanjuán, D.; Rubio, M.; Merchán, M.; Serrano-Andrés, L. *Ab initio* Determination of the Ionization Potentials of DNA and RNA Nucleobases. *J. Chem. Phys.* **2006**, *125*, No. 084302.
(24) Wolken, J. K.; Yao, C.; Tureček, F.; Polce, M. J.; Wesdemiotis, C. Cytosine Neutral Molecules and Cation-Radicals in the Gas Phase. Structures, Energetics, Ion Chemistry, and Neutralization-Reionization Mass Spectrometry. *Int. J. Mass Spectrom.* **2007**, *267*, 30−42.
(25) Zaytseva, I. L.; Trofimov, A. B.; Schirmer, J.; Plekan, O.; Feyer, V.; Richter, R.; Coreno, M.; Prince, K. C. Theoretical and Experimental Study of Valence-Shell Ionization Spectra of Guanine. *J. Phys. Chem. A* **2009**, *113*, 15142−15149.
(26) Slavíček, P.; Winter, B.; Faubel, M.; Bradforth, S. E.; Jungwirth, P. Ionization Energies of Aqueous Nucleic Acids: Photoelectron Spectroscopy of Pyrimidine Nucleosides and ab Initio Calculations. *J. Am. Chem. Soc.* **2009**, *131*, 6460−6467.
(27) Kostko, O.; Bravaya, K.; Krylov, A. I.; Ahmed, M. Ionization of Cytosine Monomer and Dimer Studied by VUV Photoionization and Electronic Structure Calculations. *Phys. Chem. Chem.* **2010**, *12*, 2860−2872.
(28) Cauët, E.; Valiev, M.; Weare, J. H. Vertical Ionization Potentials of Nucleobases in a Fully Solvated DNA Environment. *J. Phys. Chem. B* **2010**, *114*, 5886−5894.
(29) Bravaya, K.; Kostko, O.; Ahmed, M.; Krylov, A. I. The Effect of π-Stacking, H-Bonding, and Electrostatic Interactions on the Ionization Energies of Nucleic Acid Bases: Adenine−Adenine, Thymine−Thymine and Adenine−Thymine Dimers. *Phys. Chem. Chem. Phys.* **2010**, *12*, 2292−2307.
(30) Golan, A.; Bravaya, K. B.; Kudirka, R.; Kostko, O.; Leone, S. R.; Krylov, A. I.; Ahmed, M. Ionization of Dimethyluracil Dimers Leads to Facile Proton Transfer in the Absence of Hydrogen Bonds. *Nat. Chem.* **2012**, *4*, 323−329.
(31) Bravaya, K. B.; Epifanovsky, E.; Krylov, A. I. Four Bases Score a Run: Ab Initio Calculations Quantify a Cooperative Effect of H-Bonding and pi-Stacking on the Ionization Energy of Adenine in the AATT Tetramer. *J. Phys. Chem. Lett.* **2012**, *3*, 2726−2732.
(32) Schroeder, C. A.; Pluhařová, E.; Seidel, R.; Schroeder, W. P.; Faubel, M.; Slavíček, P.; Winter, B.; Jungwirth, P.; Bradforth, S. E. Oxidation Half-Reaction of Aqueous Nucleosides and Nucleotides via Photoelectron Spectroscopy Augmented by ab Initio Calculations. *J. Am. Chem. Soc.* **2015**, *137*, 201−209.
(33) Zhang, Y.; de la Harpe, K.; Beckstead, A. A.; Improta, R.; Kohler, B. UV-Induced Proton Transfer between DNA Strands. *J. Am. Chem. Soc.* **2015**, *137*, 7059−7062.
(34) Martinez-Fernandez, L.; Zhang, Y.; de la Harpe, K.; Beckstead, A. A.; Kohler, B.; Improta, R. Photoinduced Long-Lived Charge Transfer Excited States in AT-DNA Strands. *Phys. Chem. Chem. Phys.* **2016**, *18*, 21241−21245.
(35) Martinez-Fernandez, L.; Muñoz-Losa, A.; Esposito, L.; Improta, R. The Optical properties of Adenine Cation in Different Oligonucleotides: a PCM/TD-DFT Study. *Theor. Chem. Acc.* **2018**, *137*, 39.
(36) Segarra-Martí, J.; Tran, T.; Bearpark, M. J. Ultrafast and Radiationless Electronic Excited State Decay of Uracil and Thymine Cations: Computing the Effects of Dynamic Electron Correlation. *Phys. Chem. Chem. Phys.* **2019**, *21*, 14322−14330.
(37) Segarra-Marti, J.; Tran, T.; Bearpark, M. J. Computing the Ultrafast and Radiationless Electronic Excited State Decay of Cytosine and 5-Methylcytosine Cations: Uncovering the Role of Dynamic Correlation. *ChemPhotoChem* **2019**, *3*, 856−865.
(38) Tureček, F. Flying DNA Cation Radicals in the Gas Phase: Generation and Action Spectroscopy of Canonical and Noncanonical Nucleobase Forms. *J. Phys. Chem. B* **2021**, *125*, 7090−7100.
(39) Dang, A.; Nguyen, H. T. H.; Ruiz, H.; Piacentino, E.; Ryzhov, V.; Tureček, F. Experimental Evidence for Non-Canonical Thymine Cation Radicals in the Gas Phase. *J. Phys. Chem. B* **2018**, *122*, 86−97.
(40) Kim, N.-J. DFT Study of Water-Assisted Intramolecular Proton Transfer in the Tautomers of Thymine Radical Cation. *Bull. Korean Chem. Soc.* **2006**, *27*, 1009−1014.
(41) Huang, S. R.; Tureček, F. Cation Radicals of Hachimoji Nucleobases. Canonical Purine and Non-Canonical Pyrimidine Forms Generated in the Gas Phase and Characterized by UV-Vis Photodissociation Action Spectroscopy. *J. Phys. Chem. A* **2020**, *124*, 7101−7112.
(42) Huang, S. R.; Nováková, G.; Marek, A.; Tureček, F. The Elusive Non-Canonical Isomers of Ionized 9-Methyladenine and 2'-Deoxyadenosine. *J. Phys. Chem. A* **2021**, *125*, 338−348.
(43) Yates, B. F.; Bouma, W. J.; Radom, L. Distonic Radical Cations: Guidelines for the Assessment of Their Stability. *Tetrahedron* **1986**, *42*, 6225−6234.
(44) Hammerum, S. Distonic Radical Cations in Gaseous and Condensed Phase. *Mass Spectrom. Rev.* **1988**, *7*, 123−202.
(45) Adhikary, A.; Collins, S.; Khanduri, D.; Sevilla, M. D. Sugar Radicals Formed by Photoexcitation of Guanine Cation Radical in Oligonucleotides. *J. Phys. Chem. B* **2007**, *111*, 7415−7421.
(46) Choi, J.; Yang, C.; Fujitsuka, M.; Tojo, S.; Ihee, H.; Majima, T. Proton Transfer of Guanine Radical Cations Studied by Time-Resolved Resonance Raman Spectroscopy Combined with Pulse Radiolysis. *J. Phys. Chem. Lett.* **2015**, *6*, 5045−5050.
(47) Kumar, A.; Sevilla, M. D. Sugar Radical Formation by a Proton Coupled Hole Transfer in 2'-Deoxyguanosine Radical cation (2′-dG$^{\bullet+}$): A Theoretical Treatment. *J. Phys. Chem. B* **2009**, *113*, 13374−13380.
(48) Sevilla, M. D.; Kumar, A.; Adhikary, A. Comment on "Proton Transfer of Guanine Cations Studied by Time-Resolved Resonance Raman Spectroscopy Combined with Pulse Radiolysis". *J. Phys. Chem. B* **2016**, *120*, 2984−2986.
(49) Choi, J.; Yang, C.; Fujitsuka, M.; Tojo, S.; Ihee, H.; Majima, T. Reply to ″Comment on 'Proton Transfer of Guanine Cations Studied by Time-Resolved Resonance Raman Spectroscopy Combined with Pulse Radiolysis″. *J. Phys. Chem. B* **2016**, *120*, 2987−2989.
(50) Řezáč, J. Cuby: an Integrative Framework for Computational Chemistry. *J. Comput. Chem.* **2016**, *37*, 1230−1237.
(51) Řezáč, J. Cuby−ruby Framework for Computational Chemistry; Version 4, http://cuby4.molecular.cz; accessed July 2021.
(52) Nguyen, H. T. H.; Andrikopoulos, P. C.; Rulíšek, L.; Shaffer, C. J.; Tureček, F. Photodissociative Cross Linking of Noncovalent Peptide-Peptide Ion Complexes in the Gas Phase. *J. Am. Soc. Mass Spectrom.* **2018**, *29*, 1706−1720.
(53) Řezáč, J.; Fanfrlík, J.; Salahub, D.; Hobza, P. Semiempirical Quantum Chemical PM6 Method Augmented by Dispersion and H-Bonding Correction Terms Reliably Describes Various Types of Noncovalent Complexes. *J. Chem. Theory Comput.* **2009**, *5*, 1749−1760.
(54) Berendsen, H. J. C.; Postma, J. P. M.; van Gunsteren, W. F.; DiNola, A. R. H. J.; Haak, J. R. Molecular Dynamics with Coupling to an External Bath. *J. Chem. Phys.* **1984**, *81*, 3684−3690.
(55) Stewart, J. J. P. *MOPAC 16*. Stewart Computational Chemistry; Colorado Springs, CO, 2016.
(56) Becke, A. D. A New Mixing of Hartree-Fock and Local Density-Functional Theories. *J. Chem. Phys.* **1993**, *98*, 1372−1377.
(57) Zhao, Y.; Truhlar, D. G. The M06 Suite of Density Functionals for Main Group Thermochemistry, Thermochemical Kinetics, Noncovalent Interactions, Excited States, and Transition Elements: Two New Functionals and Systematic Testing of Four M06-Class

https://doi.org/10.1021/acs.jpca.2c00894
J. Phys. Chem. A 2022, 126, 2480−2497

Functionalsand 12 Other Functionals. *Theor. Chem. Acc.* **2008**, *120*, 215−241.
(58) Ayala, P. Y.; Schlegel, H. B. Identification and Treatment of Internal Rotation in Normal Mode Vibrational Analysis. *J. Chem. Phys.* **1998**, *108*, 2314−2325.
(59) Dunning, T. H., Jr. Gaussian Basis Sets for Use in Correlated Molecular Calculations. I. The Atoms Boron through Neon and Hydrogen. *J. Chem. Phys.* **1989**, *90*, 1007−1023.
(60) Schlegel, H. B. Potential Energy Curves Using Unrestricted Møller-Plesset Perturbation Theory with Spin Annihilation. *J. Chem. Phys.* **1986**, *84*, 4530−4534.
(61) Mayer, I. Spin-Projected EHF Method. IV. Comparison of Potential Curves Given by Different One-Electron Methods. *Adv. Quantum Chem.* **1978**, *14*, 29−38.
(62) Halkier, A.; Helgaker, T.; Jørgensen, P.; Klopper, W.; Koch, H.; Olsen, J.; Wilson, A. K. Basis-Set Convergence in Correlated Calculations on Ne, N_2, and H_2O. *Chem. Phys. Lett.* **1998**, *286*, 243−252.
(63) Žížek, J. On the Use of the Cluster Expansion and the Technique of Diagrams in Calculations of Correlation Effects in Atoms and Molecules. *Adv. Chem. Phys.* **1969**, *14*, 35−89.
(64) Purvis, G. D., III; Bartlett, R. J. A Full Coupled-Cluster Singles and Doubles Model: the Inclusion of Disconnected Triples. *J. Chem. Phys.* **1982**, *76*, 1910−1918.
(65) Helgaker, T.; Klopper, W.; Koch, H.; Noga, J. Basis-Set Convergence of Correlated Calculations on Water. *J. Chem. Phys.* **1997**, *106*, 9639−9646.
(66) Reed, A. E.; Weinstock, R. B.; Weinhold, F. Natural Population Analysis. *J. Chem. Phys.* **1985**, *83*, 735−746.
(67) Tomasi, J.; Mennucci, B.; Cammi, R. Quantum Mechanical Continuum Solvation Models. *Chem. Rev.* **2005**, *105*, 2999−3093.
(68) Frisch, M. J.; Trucks, G. W.; Schlegel, H. B.; Scuseria, G. E.; Robb, M. A.; Cheeseman, J. R.; Scalmani, G.; Barone, V.; Petersson, G. A.; Nakatsuji, H.; et al. *Gaussian 16, Revision A03*; Gaussian, Inc.: Wallingford, CT, 2016.
(69) Wu, R. R.; Yang, B.; Berden, G.; Oomens, J.; Rodgers, M. T. Gas-Phase Conformations and Energetics of Protonated 2′-Deoxyadenosine and Adenosine: IRMPD Action Spectroscopy and Theoretical Studies. *J. Phys. Chem. B* **2015**, *119*, 2795−2805.
(70) Tureček, F.; Havlas, Z. Thermochemistry of Unstable Enols: The O-(C_d)(H) Group Equivalent. *J. Org. Chem.* **1986**, *51*, 4066−4067.
(71) Bouchoux, G. Keto-enol tautomers and distonic ions: the Chemistry of $[C_nH_{2n}O]$ Radical Cations. Part I. *Mass Spectrom. Rev.* **1988**, *7*, 1−39.
(72) Apeloig, Y. Theoretical Calculations. In *The Chemistry of Enols*, Rappoport, Z.; ed.; John Wiley & Sons: Chichester, 1990; Chapter 1, pp. 2−74.
(73) Tureček, F. The Chemistry of Ionized Enols. In *The Chemistry of Enols*, Rappoport, Z.; ed.; John Wiley & Sons: Chichester, 1990; Chapter 3, pp. 95−146.
(74) Dang, A.; Liu, Y.; Tureček, F. UV-Vis Action Spectroscopy of Guanine, 9-Methylguanine and 2'-Deoxyguanosine Cation Radicals in the Gas Phase. *J. Phys. Chem. A* **2019**, *123*, 3272−3284.
(75) Hanus, M.; Ryjácek, F.; Kabelác, M.; Kubar, T.; Bogdan, T. V.; Trygubenko, S. A.; Hobza, P. Correlated ab Initio Study of Nucleic Acid Bases and Their Tautomers in the Gas Phase, in a Microhydrated Environment and in Aqueous Solution. Guanine: Surprising Stabilization of Rare Tautomers in Aqueous Solution. *J. Am. Chem. Soc.* **2003**, *125*, 7678−7688.
(76) Karton, A. Thermochemistry of Guanine Tautomers Re-Examined by Means of High-Level CCSD(T) Composite Ab Initio Methods. *Aust. J. Chem.* **2019**, *72*, 607−613.
(77) Wu, R. R.; Yang, B.; Berden, G.; Oomens, J.; Rodgers, M. T. Gas-Phase Conformations and Energetics of Protonated 2′-Deoxyguanosine and Guanosine: IRMPD Action Spectroscopy and Theoretical Studies. *J. Phys. Chem. B* **2014**, *118*, 14774−14784.
(78) Colominas, C.; Luque, F. J.; Orozco, M. Tautomerism and Protonation of Guanine and Cytosine. Implications in the Formation of Hydrogen-Bonded Complexes. *J. Am. Chem. Soc.* **1996**, *118*, 6811−6821.
(79) Tóth, Z.; Kubečka, J.; Muchová, E.; Slavíček, P. Ionization Emergies in Solution with QM:QM Approach. *Phys. Chem. Chem. Phys.* **2020**, *22*, 10550−10560.
(80) Kumar, A.; Sevilla, M. D. Proton Transfer Induced SOMO-to-HOMO Level Switching in One-Electron Oxidized A-T and G-C Base Pairs: A Density Functional Theory Study. *J. Phys. Chem. B* **2014**, *118*, 5453−5458.
(81) Huang, S. R.; Dang, A.; Tureček, F. Ground and Excited States of Gas-Phase DNA Nucleobase Cation-Radicals. A UV-Vis Photodisociation Action Spectroscopy and Computational Study of Adenine and 9-Methyladenine. *J. Am. Soc. Mass Spectrom.* **2020**, *31*, 1271−1281.
(82) Huang, S. R.; Tureček, F. Cation Radicals of Hachimoji Nucleobases P and Z. Generation in the Gas Phase and Characterization by UV-Vis Photodissociation Action Spectroscopy and Theory. *J. Am. Soc. Mass Spectrom.* **2021**, *32*, 373−386.
(83) Liu, Y.; Ma, C.; Nováková, G.; Marek, A.; Tureček, F. Charge-Tagged Nucleosides in the Gas Phase: UV-Vis Action Spectroscopy and Structures of Cytidine Cations, Dications, and Cation Radicals. *J. Phys. Chem. A* **2021**, *125*, 6096−6108.
(84) Liu, Y.; Dang, A.; Urban, J.; Tureček, F. Charge-Tagged DNA Radicals in the Gas Phase Characterized by UV-Vis Photodissociation Action Spectroscopy. *Angew. Chem. Int. Ed.* **2020**, *59*, 7772−7777.
(85) Korn, J. A.; Urban, J.; Dang, A.; Nguyen, H. T. H.; Tureček, F. UV-Vis Action Spectroscopy Reveals a Conformational Collapse in Hydrogen-Rich Dinucleotide Cation Radicals. *J. Phys. Chem. Lett.* **2017**, *8*, 4100−4107.
(86) Liu, Y.; Korn, J. A.; Dang, A.; Tureček, F. Hydrogen-Rich Cation Radicals of DNA Dinucleotides. Generation and Structure Elucidation by UV-Vis Action Spectroscopy. *J. Phys Chem. B* **2018**, *122*, 9665−9680.
(87) Liu, Y.; Korn, J. A.; Tureček, F. UV-Vis Action Spectroscopy and Structures of Hydrogen-Rich 2'-Deoxycytidine Dinucleotide Cation Radicals. A Difficult Case. *Int. J. Mass Spectrom.* **2019**, *443*, 22−31.
(88) Huang, S. R.; Liu, Y.; Tureček, F. UV-Vis Photodissociation Action Spectroscopy Reveals Cytosine-Guanine Hydrogen Transfer in DNA Tetranucleotide Cation Radicals upon One-Electron Reduction. *J. Phys. Chem. B* **2020**, *124*, 3505−3517.
(89) Liu, Y.; Huang, S. R.; Tureček, F. Guanine-Adenine Interactions in DNA Tetranucleotide Cation Radicals Revealed by UV/Vis Photodissociation Action Spectroscopy and Theory. *Phys. Chem. Chem. Phys.* **2020**, *22*, 16831−16842.
(90) Feketeová, L.; Chan, B.; Khairallah, G. N.; Steinmetz, V.; Maitre, P.; Radom, L.; O'Hair, R. A. J. Watson-Crick Base Pair Radical Cation as a Model for Oxidative Damage in DNA. *J. Phys. Chem. Lett.* **2017**, *8*, 3159−3165.

https://doi.org/10.1021/acs.jpca.2c00894
J. Phys. Chem. A 2022, 126, 2480−2497